Analytical and Numerical Analysis of Static Coulomb Formations

John F. Berryman

Thesis submitted to the Faculty of the
Virginia Polytechnic Institute and State University
in partial fulfillment of the requirements for the degree of

Master of Science
in
Aerospace Engineering

Hanspeter Schaub, Chair
Christopher D. Hall
Thomas Alan Lovell

November 16, 2005
Blacksburg, Virginia

Keywords: Coulomb Spacecraft Formation

Analytical and Numerical Analysis of Static Coulomb Formations

John F. Berryman

(ABSTRACT)

For close proximity flying on the order of 10–100 meters, Coulomb thrusting presents a promising alternative to other methods of propulsion. This clean and fuel-efficient propulsion method is being investigated for use in formation flying and virtual structures. In the latter application, the individual spacecraft assume fixed positions relative to each other through the use of Coulomb forces. In the work presented here, an analytical and numerical analysis is performed on such virtual structures. In the analytical portion, the constant, open-loop charges necessary to maintain a Hill-frame-static formation are determined for the cases of linear two- and three-spacecraft formations and for the case of equilateral triangular formations with spacecraft of equal mass. In addition, analysis is provided for the N-craft case so that the inter-craft charge products can be determined for any static formation. In the numerical portion, a genetic algorithm is employed to support the analytical results by determining formation geometries and charging schemes such that the formation craft remain static in the Hill frame in the absence of perturbation. The results of the numerical analysis include examples of static two-craft through nine-craft formations, including several formations that display a broader range of configurations than considered in previous works. Issues encountered during the numerical analysis are discussed, as well as the course of action taken to overcome these issues. Finally, a method is presented by which the genetic algorithm could be extended to take advantage of cluster computing.

Contents

List of Figures

List of Tables

Chapter 1

Introduction

Currently, the aerospace community is recognizing more and more applications for close proximity formation flying with separation distances varying between 10–100 meters. The ideas include plans for sparse aperture interferometry to provide remote surveillance of the Earth, and plans for spacecraft to circumnavigate and diagnose damaged spacecraft and repair them. However, there remain several technological and logistical obstacles before such missions can be realized. Electric propulsion, one of the more promising technologies for formation flying, has a significant draw-back for close proximity applications because this form of propulsion expels caustic ionic plumes that have the potential to damage fragile components of nearby spacecraft. Coulomb control is an alternative approach to close proximity formation control that is steadily gaining more attention. The basic premise of Coulomb control is to electrostatically charge spacecraft to different potentials and use the resulting inter-vehicular forces to control the spacecraft formation shape and size. Unlike electric propulsion systems, the Coulomb propulsion concept is essentially propellantless,[1,2] and thus there is little danger of equipment damage due to plume impingement. Coulomb control is orders of magnitude more fuel-efficient than electric propulsion systems, achieving specific impulses as high as 10^{13} seconds. To control the spacecraft charge, electric energy is used to accelerate positive ions and negative electrons so that they escape from the spacecraft. The high fuel-efficiency and dependence upon renewable energy will allow Coulomb formations to have mission lives considerably longer than electric propulsion based formations.

Most close proximity missions are not feasible with the technology currently available. Electric propulsion (EP) thrusters are presented as a candidate technology for this task; however, there are several problems associated with this method of propulsion that may ultimately prove insurmountable. The basic concept of the EP thruster is to rapidly accelerate and eject charged particles and in doing so propel the spacecraft forward. This method of propulsion has many beneficial qualities. For instance, the specific impulse I_{sp} provided by these systems takes values up to 6000 seconds. Additionally, the total mass of EP systems is often just a fraction of the mass of more traditional propulsion systems. Unfortunately,

EP systems have one significant drawback: the charged particles that they emit are caustic and tend to damage any material they contact. In single spacecraft missions, this effect is of no consequence because the propellant is discharged safely behind the spacecraft. However, when several spacecraft are in close proximity with one another, the propellant can damage the payload of neighboring craft. Also, because EP systems expel matter as a source of propulsion, the life of a mission will often be limited by the amount of propellant that can be carried aboard a spacecraft.[2]

The SCATHA mission was launched in January of 1979 with the goal to better understanding the charging environment of space.[1] Data from the SCATHA mission suggests that at High Earth Orbit (HEO), spacecraft can naturally attain high enough charges to exert milli-Newton level forces upon one another at a separation distance of a few dozen meters. Based upon these results, King and Parker proposed in Reference 1 to control relative spacecraft motion by exploiting inter-spacecraft electrostatic (Coulomb) force. By expelling either positively or negatively charged particles, the charge of a spacecraft can be controlled. Currently, the CLUSTERS mission demonstrates this technology by emitting charged particles so that the spacecraft maintain electrostatic neutrality relative to the charged plasma environment.[3] By generating different charges on spacecraft in close proximity, each craft exerts a force on all other spacecraft. This force can potentially be exploited to control the relative motion of the spacecraft and thus the formation shape.[1,2,4–6] However, unlike EP systems, Coulomb control would be essentially propellantless with equivalent I_{sp} values to control the relative motion ranging up to 10^{10}–10^{13} seconds. Further, the electric power required to achieve these I_{sp} values is often 1 Watt or less. The EP power requirements are typically orders of magnitude larger. Because only electrons or light ions are ejected, Coulomb thrusting is a clean method of relative motion propulsion with little potential for problems with plume impingement.[1,4]

Applications of Coulomb formations vary widely. One important application is sparse interferometry. King and Parker[1] discuss a novel method of achieving wide field of view interferometry using Coulomb thrusting. Using a distributed set of sensors, discrete readings are combined to form a high-resolution image. Meter-level sensing accuracy with infinite dwell time could be achieved by having sensors flying tens of meters apart at geostationary altitudes to form a sparse interferometric dish. In contrast, building a single structure with a diameter ranging from tens to hundreds of meters would be a costly and challenging endeavor. Interferometry, especially optical interferometry, require very precise alignments of the sensors. Adequately controlling the vibration and flexing modes of such large structures would be a difficult task. Instead, distributing sensors discretely in a tight formation would provide an attractive alternative. Such formations would be more robust to single sensor failures, because the formation could continue to function at a reduced capacity. Another application of the Coulomb concept is discussed in Reference 7. In this paper, the authors discuss the concept of a virtual Coulomb tether, in which a physical tether or boom between two spacecraft is replaced with an electrostatic force field. This basic concept could eventually be expanded so that entire virtual structures could be constructed using electro-

static forces rather than a physical truss system as internal support. Further applications include advanced docking mechanisms, autonomous inspection craft capable of circumnavigating a spacecraft via electrostatic forces, and sparse vehicles capable of carrying hazardous materials in tow without any physical contact through the use of inter-craft Coulomb forces.

Even though Coulomb control enjoys obvious advantages, it also suffers some drawbacks. Coulomb control is based upon the attraction and repulsion of charged bodies; for this reason, the charged plasma environment in space tends to diminish a spacecraft's influence upon other spacecraft by masking its charge. Additionally, the plasma environment of space will naturally charge a spacecraft. Significant spacecraft charging has been observed at geostationary altitudes.[8] Additionally, with Coulomb control, all forces are internal; i.e., each satellite is either pushing or pulling against the others. Therefore, the inertial linear and angular momentum of a formation can not be altered by Coulomb forces.[9,10] Finally, the dynamics of a Coulomb spacecraft are highly coupled and non-linear. For example, if the position or charge of one spacecraft is altered, the forces on *all* spacecraft are affected. Despite the difficulties inherent to Coulomb control, if the dynamics are better understood, then Coulomb control might one day be a fuel efficient, inexpensive, long lasting and dependable method for controlling close proximity formations.

Although the concept of Coulomb formation control is relatively new, there have already been several papers published that attest to its feasibility in real-life application. The initial NIAC report by King, Parker, et. al.,[1] remains one of the most comprehensive investigations of Coulomb control for spacecraft formations. This report contains a wide range of information including methods for physically implementing Coulomb control, potential applications of Coulomb formations, analytical derivations for several static and dynamic formations, and comparison of Coulomb propulsion with existing technologies. Reference 4 investigates examples of new analytical static Coulomb formations, discusses open-loop instability of such formations, and develops an orbit element difference based feedback control law to stabilize relative motion between two craft. In Reference 7, Natarajan and Schaub present a method of implementing and stabilizing a Coulomb tether. Here, a nadir-pointing, two-craft formation maintains a fixed separation distance while exploiting gravity gradient torque to stabilize the formation attitude. Necessary conditions are developed in Reference 11 for static, constant-charge, Coulomb formations. Here, a Hamiltonian formulation is used to analyze the dynamics of a Coulomb formation in a manner analogous to the analysis of a rigid body. In References 6 and 12, charge feedback control strategies are explored where a sensor craft is positioned using multiple drone craft.

The remainder of this work is divided into four chapters. Chapter 2 introduces fundamental concepts that drive the discussion in the rest of the thesis. In the material presented here are the equations of motion and static equilibrium equations for a Coulomb formation, as well as the center of mass and principal axes alignment conditions that play an important role in the analytical and numerical analyses that follow. Chapter 3 presents a progressive analysis of Coulomb formation statics starting with a two-spacecraft example and moving on to three-craft and general N-craft results. This chapter discusses circumstances of unim-

plementable formations as well as the interrelation of the static equations and formation constraints. In Chapter 4, a numerical analysis is presented that employs the genetic algorithm (GA) to search for Coulomb formations that are stationary in the Hill frame. Due to the increase in computational capacity over the past several years, the GA has become more popular for use in optimization problems. In the aerospace field alone, the GA has been applied to tasks ranging from the optimization of satellite constellations to designing low-thrust trajectories.[13–17] Since the GA is much more capable than classical optimization schemes in dealing with discontinuous cost functions with numerous local minima, it is an ideal tool for the research at hand. The results determined by the GA include both static Hill frame formations and static deep-space formations. This chapter also includes a detailed discussion of the genetic algorithm used for this research. Finally, the last chapter summarizes the results of this research and presents ideas for future study of Coulomb spacecraft formations.

Chapter 2

Problem Statement

Let $\boldsymbol{r}_i$ represent the inertial position of the i^{th} spacecraft within a formation. Also, let $\boldsymbol{r}_c$ represent the inertial position vector of the center of mass of a spacecraft formation. The position of the spacecraft relative to the formation center of mass is then $\boldsymbol{\rho}_i = \boldsymbol{r}_i - \boldsymbol{r}_c$ and the position of spacecraft i relative to spacecraft j is similarly defined as $\boldsymbol{\rho}_{ji} = \boldsymbol{\rho}_i - \boldsymbol{\rho}_j$. The Hill frame is defined as $\mathcal{H} : \{\mathcal{O}, \hat{\boldsymbol{o}}_r, \hat{\boldsymbol{o}}_\theta, \hat{\boldsymbol{o}}_h\}$, where $\hat{\boldsymbol{o}}_r$ points radially away from the center of Earth, $\hat{\boldsymbol{o}}_h$ points in the orbit-normal direction and the final unit vector $\hat{\boldsymbol{o}}_\theta$ completes the triad such that $\hat{\boldsymbol{o}}_\theta = \hat{\boldsymbol{o}}_h \times \hat{\boldsymbol{o}}_r$. For circular restricted center of mass motion considered in this research, $\hat{\boldsymbol{o}}_\theta$ is always in the direction of the velocity of the formation center of mass. As illustrated in Fig. 2.1, the i^{th} relative position vector is represented in the Hill frame vector components as

$$\boldsymbol{\rho}_i = {}^{\mathcal{H}}\begin{bmatrix} x_i \\ y_i \\ z_i \end{bmatrix} \tag{2.1}$$

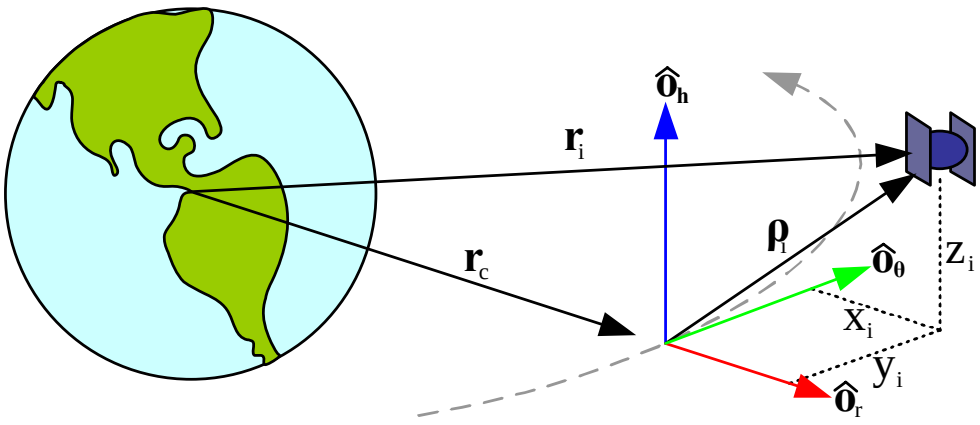

Figure 2.1: Illustration of rotating Hill coordinate frame.

Under the assumption that the formation spacecraft are point charges, if each spacecraft has a charge q_i, then the Coulomb interaction between the i^{th} and j^{th} spacecraft is proportional to the product of their charges and inversely proportional to the square of their separation distance. If the charges are of like sign, then the interaction is repulsive, otherwise it is attractive. The equations of motion for a Coulomb spacecraft formation can be found by including the massless Coulomb force term on the right side of the Hill's equations.[18–20]

$$\ddot{x}_i - 2n\dot{y}_i - 3n^2 x_i = \frac{k_c}{m_i} \sum_{j=1}^{N} \frac{x_i - x_j}{\rho_{ji}^3} q_i q_j e^{-\frac{\rho_{ij}}{\lambda_d}} \tag{2.2a}$$

$$\ddot{y}_i + 2n\dot{x}_i = \frac{k_c}{m_i} \sum_{j=1}^{N} \frac{y_i - y_j}{\rho_{ji}^3} q_i q_j e^{-\frac{\rho_{ij}}{\lambda_d}} \tag{2.2b}$$

$$\ddot{z}_i + n^2 z_i = \frac{k_c}{m_i} \sum_{j=1}^{N} \frac{z_i - z_j}{\rho_{ji}^3} q_i q_j e^{-\frac{\rho_{ij}}{\lambda_d}} \tag{2.2c}$$

In order for the spacecraft to remain fixed relative to the Hill frame, all derivatives in Eqs. (2.2) must remain zero for all time. This relative equilibrium configuration is achieved by carefully placing and charging the craft such that the Hill frame accelerations are exactly canceled by the accelerations due to Coulomb forces. In these equations, n refers to the mean orbit rate for motion of the center of mass, and k_c refers to Coulomb's constant, 8.99×10^9 Nm^2/C^2. The exponential term on the right hand side of Eqn. (2.2) dictates the rate at which the Coulomb influence decays with increasing distance in a plasma environment. This decay is a function of the Debye length, λ_d, and is due to the shielding effect that is created around a charged body when submersed in a plasma environment.

In Low Earth Orbit, LEO, the Debye length can be on the order of centimeters, rendering this method of control ineffective except at extremely close ranges, for example perturbative corrections during the final phase of docking. On the other hand, at Geosynchronous Earth Orbit, GEO, altitudes, the Debye length ranges from 140–1400 meters.[1,2] Therefore, the analysis presented in the majority of this thesis considers GEO altitude formations with spacecraft separations on the order of ten meters. With such formations, the exponential term can be disregarded, so that the analysis parallels earlier methods used by Parker and King to find analytical charge solutions.[1]

To make the analysis less complicated, the equations of motion are normalized with respect to the orbital rate, n, and Coulomb's Constant, k_c. This normalization is accomplished by introducing a normalized charge, $\tilde{q} \equiv q\sqrt{k_c}/n$. By substituting in this new variable, disregarding the exponential term and setting all derivatives to zero, the static equations for a

Coulomb formation can be written as

$$m_i \frac{\ddot{x}_i}{n^2} = 0 = 3x_i m_i + \sum_{j=1}^{N} \frac{x_i - x_j}{\rho_{ji}^3} \tilde{q}_i \tilde{q}_j \tag{2.3a}$$

$$m_i \frac{\ddot{y}_i}{n^2} = 0 = \sum_{j=1}^{N} \frac{y_i - y_j}{\rho_{ji}^3} \tilde{q}_i \tilde{q}_j \tag{2.3b}$$

$$m_i \frac{\ddot{z}_i}{n^2} = 0 = -z_i m_i + \sum_{j=1}^{N} \frac{z_i - z_j}{\rho_{ji}^3} \tilde{q}_i \tilde{q}_j \tag{2.3c}$$

If these equations are satisfied, then the Hill frame accelerations are exactly matched by the Coulomb accelerations and the spacecraft remain fixed in place with respect to the Hill frame. Notice in Eqn. (2.3) that the equations are linear in the charge products, $\tilde{q}_i \tilde{q}_j$. This fact is central to the analytical treatment, and for this reason we represent the charge products as Q_{ij} as follows

$$Q_{ij} \equiv \tilde{q}_i \tilde{q}_j \tag{2.4}$$

A hill-frame static formation must satisfy two conditions. The first condition is that the formation center of mass must be located at the origin of the hill frame and the second is that the principal axes of the formation must be aligned with the axes of the hill frame.

First, the center of mass condition is considered. If the formation remains rigid, then the center of mass of the formation moves according to Hill's equations as presented in Eqn. (2.2), except that there is no forcing function and the right hand side of the equation is therefore zero. Solving for the center of mass accelerations and prescribing the velocities to be zero yields

$$\ddot{x}_{\text{cm}} = 3n^2 x_{\text{cm}} \tag{2.5a}$$

$$\ddot{y}_{\text{cm}} = 0 \tag{2.5b}$$

$$\ddot{z}_{\text{cm}} = -n^2 z_{\text{cm}} \tag{2.5c}$$

From Eqs. (2.5), it is apparent that if the center of mass is placed some distance away from the origin in the $\hat{\boldsymbol{o}}_r$ or $\hat{\boldsymbol{o}}_h$ directions, there is an associated acceleration and the center of mass does not remain stationary. On the other hand, from Eqn. (2.5b), if the center of mass is positioned some distance away from the origin in the $\hat{\boldsymbol{o}}_\theta$ direction, there is no associated acceleration and the center of mass remains stationary. However, such a formation is not unique. By simply defining a new Hill frame with an origin offset y_{cm} from the original Hill frame, the original formation center of mass coincides with the origin of the new Hill frame. Therefore, in order to establish a unique formation, the center of mass may not be offset in the $\hat{\boldsymbol{o}}_\theta$ direction. The center of mass condition is expressed mathematically as

$$M\bar{\boldsymbol{\rho}} = \sum_{i=1}^{N} m_i \boldsymbol{\rho}_i = \sum_{i=1}^{N} m_i \begin{bmatrix} x_i \\ y_i \\ z_i \end{bmatrix} = \mathbf{0} \tag{2.6}$$

where M is the total mass of the formation, $\bar{\boldsymbol{\rho}}$ is the position vector from the spacecraft to the center of mass, and all vector components are expressed in the Hill frame.

The principal axes condition is now considered. In a static Coulomb formation, the internal forces hold the spacecraft fixed relative to one another. It is therefore possible to apply the theory of rigid body dynamics to the analysis of this system. Euler's equation is the fundamental equation of rotational dynamics

$$[I]\,\dot{\boldsymbol{\omega}} = -\boldsymbol{\omega} \times [I]\,\boldsymbol{\omega} + \mathbf{g} \tag{2.7}$$

where $\boldsymbol{\omega}$ is the rigid body angular velocity vector, $[I]$ is the inertia tensor, and $\mathbf{g}$ is the external torque applied to the rigid body. In order for a formation to remain static in the Hill frame, the rotation of a formation relative to the Hill frame must be zero, or $\boldsymbol{\omega}_{\mathcal{F}/\mathcal{H}} = \mathbf{0}$. Furthermore, the rotation of the Hill frame relative to the inertia perifocal frame is $\boldsymbol{\omega}_{\mathcal{H}/\mathcal{P}} = n\hat{\boldsymbol{o}}_h$, where n is the mean orbital rate. Therefore the rotation of the formation with respect to the perifocal frame is

$$\boldsymbol{\omega}_{\mathcal{F}/\mathcal{P}} = \boldsymbol{\omega}_{\mathcal{F}/\mathcal{H}} + \boldsymbol{\omega}_{\mathcal{H}/\mathcal{P}} = \mathbf{0} + n\hat{\boldsymbol{o}}_h \tag{2.8}$$

Henceforth, the only rotational velocity that is considered is that of the formation with respect to the perifocal frame, so that the subscripts are no longer necessary:

$$\boldsymbol{\omega} \equiv \boldsymbol{\omega}_{\mathcal{F}/\mathcal{P}} = n\hat{\boldsymbol{o}}_h \tag{2.9}$$

Expressed in the perifocal frame *or* Hill frame, $\boldsymbol{\omega}$ is represented as

$${}^{\mathcal{P}}\boldsymbol{\omega} = {}^{\mathcal{H}}\boldsymbol{\omega} = \begin{bmatrix} 0 \\ 0 \\ n \end{bmatrix} \tag{2.10}$$

Since $\boldsymbol{\omega}$ is constant as seen in Eqn. (2.9), $\dot{\boldsymbol{\omega}}$ must therefore be zero.

In Reference 20 it is shown that an object orbiting the Earth will experience a gravity gradient torque $\mathbf{L}_G$ of the form

$$\mathbf{L}_G = \frac{3n^2}{r_c^2}\mathbf{r}_c \times [I]\,\mathbf{r}_c \tag{2.11}$$

where, $\mathbf{r}_c$ is the vector that points from the center of the Earth to the center of mass of the rigid formation. As represented in the Hill frame

$$\mathbf{r}_c = {}^{\mathcal{H}}\begin{bmatrix} r_c \\ 0 \\ 0 \end{bmatrix} \tag{2.12}$$

Since the formation does not move with respect to the Hill frame, the Hill-frame representation of the formation inertia matrix is constant and can be defined as

$$[I] \equiv {}^{\mathcal{H}}\begin{bmatrix} I_{xx} & I_{xy} & I_{xz} \\ I_{xy} & I_{yy} & I_{yz} \\ I_{xz} & I_{yz} & I_{zz} \end{bmatrix} \tag{2.13}$$

Finally, the Hill frame is related to the perifocal frame by a rotation f about the $\hat{\boldsymbol{o}}_h$ axis as represented in the following matrix.

$$[R_{\mathcal{P}/\mathcal{H}}] = \begin{bmatrix} \cos f & \sin f & 0 \\ -\sin f & \cos f & 0 \\ 0 & 0 & 1 \end{bmatrix} \tag{2.14}$$

Now there is enough information to represent Eqn. (2.7) in the perifocal frame.

$$\begin{aligned} [I]\,\dot{\boldsymbol{\omega}} = \mathbf{0} &= -\boldsymbol{\omega} \times [I]\,\boldsymbol{\omega} + \mathbf{L}_G \\ &= -{}^{\mathcal{P}}\boldsymbol{\omega} \times [R_{\mathcal{P}/\mathcal{H}}]^{\mathcal{H}}\,[I]\,[R_{\mathcal{P}/\mathcal{H}}]^{T\,\mathcal{P}}\boldsymbol{\omega} \\ &\quad + \frac{3n^2}{R_c^2}[R_{\mathcal{P}/\mathcal{H}}]^{\mathcal{H}}\mathbf{R}_c \times [R_{\mathcal{P}/\mathcal{H}}]^{\mathcal{H}}\,[I]\,{}^{\mathcal{H}}[R_{\mathcal{P}/\mathcal{H}}]^T[R_{\mathcal{P}/\mathcal{H}}]\mathbf{R}_c \\ &= -{}^{\mathcal{P}}\boldsymbol{\omega} \times [R_{\mathcal{P}/\mathcal{H}}]^{\mathcal{H}}\,[I]\,{}^{\mathcal{P}}\boldsymbol{\omega} \\ &\quad + \frac{3n^2}{R_c^2}[R_{\mathcal{P}/\mathcal{H}}]^{\mathcal{H}}\mathbf{R}_c \times [R_{\mathcal{P}/\mathcal{H}}]^{\mathcal{H}}\,[I]\,{}^{\mathcal{H}}\mathbf{R}_c \\ \begin{bmatrix} 0 \\ 0 \\ 0 \end{bmatrix} &= \begin{bmatrix} -4n^2 I_{31}\sin f + n^2 I_{23}\cos f \\ -4n^2 I_{31}\cos f - n^2 I_{23}\sin f \\ 3n^2 I_{12} \end{bmatrix} \end{aligned} \tag{2.15}$$

Therefore, the only way for $\dot{\boldsymbol{\omega}}$ to be zero for all time is for the Hill frame representation of the products of inertia to be zero, $I_{xy} = I_{yz} = I_{zx} = 0$, or equivalently, for the principal axes to be aligned with the Hill frame axes. The following equations mathematically express that the products of inertia are zero:

$$I_{xy} = -\sum_{i=1}^{N} m_i x_i y_i = 0 \tag{2.16a}$$

$$I_{yz} = -\sum_{i=1}^{N} m_i y_i z_i = 0 \tag{2.16b}$$

$$I_{zx} = -\sum_{i=1}^{N} m_i z_i x_i = 0 \tag{2.16c}$$

Although less rigorous, an alternative rationale for the necessity of principal axes alignment provides additional insight. In order to eliminate gravity gradient torque, one of the principal axes of the rigid formation must be aligned with the $\hat{\boldsymbol{o}}_r$ direction and in order for the formation to rotate with a constant rotational velocity of $n\hat{\boldsymbol{o}}_h$, one of the principal axes of the formation must be aligned with the $\hat{\boldsymbol{o}}_h$ direction. Since two of the principal axes are aligned with two of the Hill frame axes, the third principal axis is automatically aligned with the third Hill frame axis as well.

In summary, in order to maintain a unique, static formation in the Hill frame, it has been shown that the formation center of mass must be located at the origin of the Hill frame

and the formation principal axes must be aligned with the Hill frame axes. These conditions are crucial in the analytical and numerical studies to follow.

Chapter 3

Closed-Form Analysis

If Coulomb formation flight is ever to be employed in actual space missions, the dynamics must be more clearly understood. As an additional step in this direction, this chapter presents an closed-form analysis of Coulomb formation statics. Initially, the simple case of a two-craft formation will be considered. After discussing all possible two-spacecraft formations, the analysis continues with all possible linear three-craft cases and the special planar three-craft case of an equilateral triangle formation with spacecraft of equal masses. Finally a method is outlined by which the charge products, Q_{ij}, can be determined for an arbitrary formation of N craft. However, the fact that the charge products can always be determined in no way indicates that constant charges can be found to implement the formation. To this end, cases where a formation can not be implemented with constant charges are thoroughly discussed.

3.1 Analysis of a Two-Spacecraft Formation

This section provides an analysis of a static formation of two spacecraft. The analysis of this section also serves as a tutorial for a new notational convention used through the remainder of this chapter. The new notation decreases work necessary for the analysis by allowing several cases to be considered simultaneously.

3.1.1 Two-Spacecraft Formation Aligned with $\hat{\boldsymbol{o}}_r$ Axis

Figure 3.1 shows two spacecraft aligned with the $\hat{\boldsymbol{o}}_r$ axis. They are separated by a distance L and in accordance with the center of mass condition, the formation center of mass is located at the origin. Using the center of mass condition, the position of the second mass can be

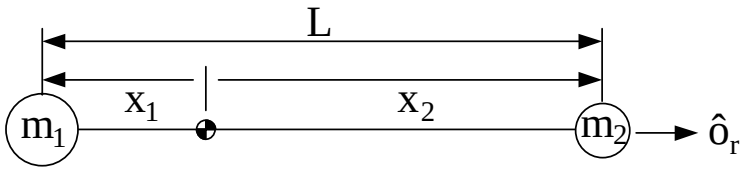

Figure 3.1: Two-spacecraft formation aligned with the $\hat{\boldsymbol{o}}_r$ axis.

expressed in terms of the first mass's position.

$$x_2 = -\frac{m_1}{m_2} x_1 \tag{3.1}$$

The separation distance is then expressed in terms of the first position as

$$L = x_2 - x_1 = -x_1 \left(1 + {}^{m_1}\!/_{m_2}\right) \tag{3.2}$$

According to the Hill equation for $\hat{\boldsymbol{o}}_r$ alignment, Eqn. (2.3a), there are two equations that must be satisfied to assure that the formation is frozen in the Hill frame, one equation for each spacecraft:

$$-3x_1 = \frac{1}{m_1} \frac{x_1 - x_2}{L^3} \tilde{q}_1 \tilde{q}_2 = -\frac{Q_{12}}{m_1 L^2} \tag{3.3a}$$

$$-3x_2 = \frac{1}{m_2} \frac{x_2 - x_1}{L^3} \tilde{q}_1 \tilde{q}_2 = \frac{Q_{12}}{m_2 L^2} \tag{3.3b}$$

where $Q_{ij} \equiv \tilde{q}_i \tilde{q}_j$. By substituting the center of mass condition of Eqn. (3.1) into Eqn. (3.3b) it is trivial to show that Eqn. (3.3b) is redundant, and Eqn. (3.3a) is then the only necessary condition. Solving this equation for Q_{12} yields[21]

$$Q_{12} = 3 m_1 x_1 L^2 = 3 m_1 x_1^3 \left(1 + {}^{m_1}\!/_{m_2}\right)^2 \tag{3.4}$$

If the spacecraft are charged and placed such that the above equation is satisfied, then the formation remains stationary in the Hill frame.

3.1.2 Introduction of New Notation

In Section 3.1.1, a charge solution is found for a two-spacecraft Coulomb formation aligned with the $\hat{\boldsymbol{o}}_r$ axis. Initially, it may seem that similar solutions can be found for arbitrary placement of two spacecraft as long as the center of mass condition is satisfied. However, as discussed in Chapter 1, in order to maintain a static Coulomb formation, the formation principal axes must be aligned with the axes of the Hill frame. Since the principal axis of the two-craft formation is aligned with the craft themselves, it is only necessary to examine

the cases where the two spacecraft are aligned with one of the coordinate axes of the Hill frame. Furthermore, rather than replicating the analysis of Sect. 3.1.1, a notational system is introduced that allows the simultaneous solution for all possible two-spacecraft alignments.

Instead of examining positions x_i along the $\hat{\boldsymbol{o}}_r$ axis, the premise of the following notational system is to examine positions d_i along an unspecified axis $\hat{\boldsymbol{o}}_1$ that can be chosen from $\hat{\boldsymbol{o}}_r$, $\hat{\boldsymbol{o}}_\theta$, or $\hat{\boldsymbol{o}}_h$. Using this notation, Eqs. (2.3) can be rewritten as

$$a_d d_i = \frac{1}{m_i} \sum_{j=1}^{N} \frac{d_i - d_j}{\rho_{ji}^3} \tilde{q}_i \tilde{q}_j \tag{3.5}$$

Where a_d is a constant that depends upon the choice of d. If $d = x$, then $a_d = a_x = -3$; if $d = y$, then $a_d = a_y = 0$; finally, if $d = z$, then $a_d = a_z = 1$. This equation is equivalent to Eqs. (2.3) yet it allows the direction in which distances are measured to remain arbitrary. Using this notation, Eqn. (3.5) can be solved for the charge products, Q_{ij}. By then supplying the appropriate value for the constant, a_d, the results can then be specified for a two-craft formation aligned with any Hill frame axis.

3.1.3 Two-Spacecraft Formation Aligned with Any Hill-Frame Axis

Because an analysis has already been performed for two spacecraft aligned with the $\hat{\boldsymbol{o}}_r$ axis, this section presents a truncated version of the general analysis for two spacecraft aligned with any Hill frame axis.

Making use of the notation just presented, the necessary condition represented in Eqn. (3.3a) can be generalized to

$$a_d d_1 = \frac{1}{m_1} \frac{d_1 - d_2}{L^3} \tilde{q}_1 \tilde{q}_2 = -\frac{Q_{12}}{m_1 L^2} \tag{3.6}$$

Solving for the charge product yields

$$Q_{12} = -a_d m_1 d_1 L^2 = -a_d m_1 d_1^3 \left(1 + {}^{m_1}\!/_{m_2}\right)^2 \tag{3.7}$$

Several conclusions can be drawn from this general equation by substituting in values for the constant a_d. If the formation is aligned with the $\hat{\boldsymbol{o}}_r$ axis, then $a_d = a_x = -3$. Because d_1 is always negative, Q_{12} is negative and both spacecraft must be charged with opposite polarity. For the $\hat{\boldsymbol{o}}_\theta$ aligned case, $a_d = a_y = 0$; therefore at least one craft must have zero charge so that there is no interaction between the two spacecraft. This formation corresponds to a leader-follower spacecraft formation, and any inter-spacecraft forces would obviously disrupt such a formation. Finally, if the spacecraft are aligned with $\hat{\boldsymbol{o}}_h$, then $a_d = a_z = 1$. In this case, the necessary charge product, Q_{12}, is a third of the charge product required for the $\hat{\boldsymbol{o}}_r$ aligned case; additionally, the spacecraft must be charged to the same polarity to support

a stationary formation. The rationale behind this charging scheme can be understood by imagining the motion of two bodies whose orbits differ only in inclination. With no charge, the spacecraft would collide when they reached the equatorial plane; however when charged to the same polarity they push one another apart and do not collide.

Coulomb formations of two spacecraft are the simplest possible formations. Such formations will find utility as virtual tethers between two spacecraft[7] and for applications such as rendezvous and docking.

3.2 Analysis of Linear Three-Spacecraft Formation

The same methodology is now applied to the analysis of a formation composed of three collinear spacecraft. Due to the principal axis constraint, linear formations must always be aligned with one of the three Hill-frame axes.

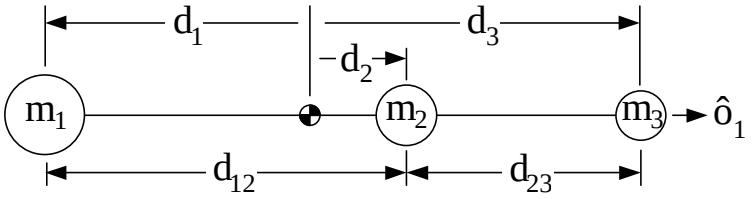

Figure 3.2: Three-spacecraft formation aligned with an arbitrary axis.

Figure 3.2 illustrates a linear three-craft formation aligned with an arbitrary axis. The spacecraft are positioned along the axis at locations d_1, d_2, and d_3, with separations of d_{12} and d_{23}. For this formation, Eqn. (3.5) is re-written as three necessary conditions for a stationary formation:

$$a_d d_1 m_1 = \frac{d_1 - d_2}{d_{12}^3} Q_{12} + \frac{d_1 - d_3}{d_{13}^3} Q_{13} = -\frac{Q_{12}}{d_{12}^2} - \frac{Q_{13}}{d_{13}^2} \tag{3.8a}$$

$$a_d d_2 m_2 = \frac{d_2 - d_1}{d_{12}^3} Q_{12} + \frac{d_2 - d_3}{d_{23}^3} Q_{23} = \frac{Q_{12}}{d_{12}^2} - \frac{Q_{23}}{d_{23}^2} \tag{3.8b}$$

$$a_d d_3 m_3 = \frac{d_3 - d_2}{d_{23}^3} Q_{23} + \frac{d_3 - d_1}{d_{13}^3} Q_{13} = \frac{Q_{23}}{d_{23}^2} + \frac{Q_{13}}{d_{13}^2} \tag{3.8c}$$

Notice that Eqs. (3.8) are linear in the charge products Q_{ij}. Adding Eqn. (3.8a) and Eqn. (3.8c) and substituting in the center of mass definition produces an equation identical to Eqn. (3.8a). In effect, there are three variables available for control and only two independent necessary conditions. Therefore one of the charge products, Q_{13} for example, may be chosen arbitrarily while the other charge products can be solved for from Eqs. (3.8a)

and (3.8c):

$$Q_{12} = \left[-a_d d_1 m_1 - \frac{Q_{13}}{d_{13}^2} \right] d_{12}^2 \tag{3.9a}$$

$$Q_{23} = \left[a_d d_3 m_3 - \frac{Q_{13}}{d_{13}^2} \right] d_{23}^2 \tag{3.9b}$$

By considering the center of mass constraint, these equations are conveniently rewritten in terms of separation distances

$$Q_{12} = \left[\frac{a_d m_1}{M} \left(d_{12} \left(m_2 + m_3 \right) + d_{23} \left(m_3 \right) \right) - \frac{Q_{13}}{d_{13}} \right] d_{12}^2 \tag{3.10a}$$

$$Q_{23} = \left[\frac{a_d m_3}{M} \left(d_{12} \left(m_1 \right) + d_{23} \left(m_1 + m_2 \right) \right) - \frac{Q_{13}}{d_{13}} \right] d_{23}^2 \tag{3.10b}$$

where M is the total formation mass. With these equations it is possible to determine the charge products necessary for a stationary, linear three-craft formation. However, it must be noted that while it is always be possible to determine the charge products Q_{ij}, it is not always be possible to determine suitable charges, $\tilde{q}_i$. Using $Q_{ij} = \tilde{q}_i \tilde{q}_j$, for a three-craft formation the individual charges are determined by

$$\tilde{q}_i = \sqrt{\left(\frac{Q_{ij} Q_{ik}}{Q_{jk}} \right)} \tag{3.11}$$

Equation (3.11) implies two important qualities that must be exhibited by the charge products.

1. In order for the charges to be real quantities, the term under the radical must not be negative. However, rather than ensuring that $Q_{12}Q_{13}/Q_{23}$, $Q_{12}Q_{23}/Q_{13}$, and $Q_{13}Q_{23}/Q_{12}$ are not negative, it is equivalent and less difficult to simply ensure that the triple product $Q_{12}Q_{23}Q_{13}$ is non-negative.

2. In order for charge magnitudes to be finite, the value of $Q_{ij}Q_{jk}/Q_{ik}$ must be finite. Therefore it is not possible to have a static formation when a single charge product Q_{ij} is zero because the denominator would be zero and the value for one of the charges $\tilde{q}_i$ would be infinite. However, because there are two charge products in the numerator, a static formation is still possible when either two or three charge products have zero value.

It should be possible to implement any linear three-spacecraft formation; however the charge product, Q_{13}, must be carefully chosen so that these conditions are fulfilled. Just as in the case of two-spacecraft Coulomb formations, three-spacecraft formations may be used as virtual tethers, however there currently exists no extensive stability or control analysis as in the case of nadir-pointing two-spacecraft formations.

3.3 Analysis of Triangular Three-Spacecraft Formations

3.3.1 Arbitrary Triangle Formation

An arbitrary, triangular three-spacecraft formation must satisfy the conditions of Eqs. (2.3) in order to remain stationary in the Hill frame. These equations state the conditions necessary for each craft to remain motionless in the $\hat{\boldsymbol{o}}_r$, $\hat{\boldsymbol{o}}_\theta$, and $\hat{\boldsymbol{o}}_h$ directions. These equations can be immediately reduced to six equations by recognizing that a three-craft formation is inherently planar and that a principal axis of any planar formation is perpendicular to the plane of the formation. Therefore in order to satisfy the principal axes condition, the three spacecraft must lie in one of the three planes that are perpendicular to the Hill frame axes. Since the formation spacecraft are constrained to lie in a plane spanned by two of the Hill frame axes, it is unnecessary include equations concerning motion perpendicular to this plane. The position of each spacecraft is then specified by two values: a distance d_i in the $\hat{\boldsymbol{o}}_1$ direction, and a distance e_i in the $\hat{\boldsymbol{o}}_2$ direction where $\hat{\boldsymbol{o}}_1$ and $\hat{\boldsymbol{o}}_2$ can be defined as any combination of the directions $\hat{\boldsymbol{o}}_r$, $\hat{\boldsymbol{o}}_\theta$, and $\hat{\boldsymbol{o}}_h$. The remaining equations that must be satisfied in order for the spacecraft to remain static are

$$m_i\frac{\ddot{d}_1}{n^2} = 0 = a_d m_1 d_1 + \frac{d_1-d_2}{\rho_{12}^3}Q_{12} + \frac{d_1-d_3}{\rho_{13}^3}Q_{13} \tag{3.12a}$$

$$m_i\frac{\ddot{d}_2}{n^2} = 0 = a_d m_2 d_2 + \frac{d_2-d_1}{\rho_{12}^3}Q_{12} + \frac{d_2-d_3}{\rho_{23}^3}Q_{23} \tag{3.12b}$$

$$m_i\frac{\ddot{d}_3}{n^2} = 0 = a_d m_3 d_3 + \frac{d_3-d_1}{\rho_{13}^3}Q_{13} + \frac{d_3-d_2}{\rho_{23}^3}Q_{23} \tag{3.12c}$$

$$m_i\frac{\ddot{e}_1}{n^2} = 0 = a_e m_1 e_1 + \frac{e_1-e_2}{\rho_{12}^3}Q_{12} + \frac{e_1-e_3}{\rho_{13}^3}Q_{13} \tag{3.12d}$$

$$m_i\frac{\ddot{e}_2}{n^2} = 0 = a_e m_2 e_2 + \frac{e_2-e_1}{\rho_{12}^3}Q_{12} + \frac{e_2-e_3}{\rho_{23}^3}Q_{23} \tag{3.12e}$$

$$m_i\frac{\ddot{e}_3}{n^2} = 0 = a_e m_3 e_3 + \frac{e_3-e_1}{\rho_{13}^3}Q_{13} + \frac{e_3-e_2}{\rho_{23}^3}Q_{23} \tag{3.12f}$$

As a reminder, the first derivatives are not included in these equations because they can be prescribed, and are always zero for a static formation. Also, the constants a_d and a_e are used to maintain generality and can be replaced by either -3, 0, or 1 depending upon the axial alignment of the formation. For instance, if the formation lies in the plane spanned by the vectors $\hat{\mathbf{o}}_r$ and $\hat{\mathbf{o}}_h$, then $a_d = a_x = -3$ and $a_e = a_z = 1$.

For an arbitrary three-craft formation, the center of mass condition applies two constraints that ensure the formation center of mass coincides with the origin of the Hill frame.

$$m_1 d_1 + m_2 d_2 + m_3 d_3 = 0 \tag{3.13a}$$

$$m_1 e_1 + m_2 e_2 + m_3 e_3 = 0 \tag{3.13b}$$

Similarly, the principal axes condition applies one more constraint to ensure that the product of inertia, I_{de} is zero. If all products of inertia are zero, then all of the formation principal axes will be aligned with the Hill frame axes. The principal axes constraint is

$$m_1 d_1 e_1 + m_2 d_2 e_2 + m_3 d_3 e_3 = 0 \tag{3.14}$$

Next we show that three of the static equations are automatically satisfied if these constraints are applied. First, the constraint represented in Eqn. (3.13a) is examined. If this constraint is applied, then the displacement of the third craft in the $\hat{\boldsymbol{o}}_1$ direction can be described by the displacements of the other craft:

$$d_3 = -\frac{m_1 d_1 + m_2 d_2}{m_3} \tag{3.15}$$

Now a question is posed: if this constraint is imposed, and the first two static equations, Eqs. (3.12a) and (3.12b), are satisfied, then is it ever possible that the static equation represented in Eqn. (3.12c) will not be satisfied? The answer can be seen by taking the second derivative of this constraint and by substituting in $\ddot{d}_1 = 0$ and $\ddot{d}_2 = 0$ from Eqs. (3.12a) and (3.12b).

$$\ddot{d}_3 = -\frac{m_1 \ddot{d}_1 + m_2 \ddot{d}_2}{m_3} = 0 \tag{3.16}$$

Therefore Eqn. (3.12c) is automatically satisfied. In this manner, the first center of mass constraint effectively eliminates Eqn. (3.12c). In exactly the same manner, the second center of mass constraint can be used to eliminate Eqn. (3.12f).

Similarly, the principal axes constraint of Eqn. (3.14) can be used to eliminate one more static equation as shown by first solving Eqn. (3.14) for d_1.

$$d_1 = -\frac{m_2 d_2 e_2 + m_3 d_3 e_3}{m_1 e_1} \tag{3.17}$$

Again a similar question is posed: if this constraint is enforced, and Eqs. (3.12b)-(3.12f) are satisfied, then is it ever possible that the static equation represented in Eqn. (3.12a) will not be satisfied? The answer is found by differentiating the constraint equation twice and then setting all of the velocities and accelerations on the right-hand side to zero, thereby signifying that Eqs. (3.12b) through (3.12f) are satisfied. The second derivative of Eqn. (3.17) is signifigantly more complex than its center of mass counterpart.

$$\ddot{d}_1 = \frac{\left(\begin{array}{l} e_1 \ddot{e}_1 \sum_{\ell=2}^{3} m_\ell d_\ell e_\ell - e_1^2 \sum_{\ell=2}^{3} m_\ell \left(\ddot{d}_\ell e_\ell + 2\dot{d}_\ell \dot{e}_\ell + d_\ell \ddot{e}_\ell \right) \\ -2\dot{e}_1^2 \sum_{\ell=2}^{3} m_\ell d_\ell e_\ell + 2 e_1 \dot{e}_1 \sum_{\ell=2}^{3} m_\ell \left(\dot{d}_\ell e_\ell + d_\ell \dot{e}_\ell \right) \end{array} \right)}{m_1 e_1^3} = 0 \tag{3.18}$$

Here the sigma notation has been used not only to save space, but also so that Eqn. (3.18) serves as a prototype for the N-spacecraft case that is discussed in Sect. 3.3.2. Since the right hand side of Eqn. (3.18) is zero when Eqs. (3.12b) through (3.12f) are satisfied, Eqn. (3.12a) is automatically satisfied. Notice that Eqn. (3.18) has a potential issue with singularity in the case that $e_1 = 0$, however, by applying l'Hospital's rule, it can be shown that in the limiting case as $e_1 \to 0$, the right hand side approaches zero. Therefore it is no longer necessary to consider Eqn. (3.12a).

The method described here uses the center of mass constraints to eliminate two equations and the principal axes constraint to eliminate one more condition. In this case Eqs. (3.12a) and (3.12c) are eliminated from the set of equations for the $\hat{\boldsymbol{o}}_1$ direction and Eqn. (3.12f) is eliminated from the set of equations for the $\hat{\boldsymbol{o}}_2$ direction. Now, only three equations remain: Eqs. (3.12b), (3.12d) and (3.12e). If the constraints are enforced, then once these equations are satisfied, Eqs. (3.12a), (3.12c) and (3.12f) are satisfied automatically. Eqs. (3.12b), (3.12d) and (3.12e) are linear in charge products, Q_{12}, Q_{13}, and Q_{23}, therefore the values of the charge products can be easily determined. However, as discussed at the end of section 3.2, even though the charge products, Q_{ij}, can always be found, this does not guarantee that appropriate charges, $\tilde{q}_i$, can be found.

3.3.2 Equilateral Triangle Formation

The analysis just presented for arbitrary triangular formations is applicable for the specific case of an equilateral triangle formation. In this formation, each craft is assumed to have the same mass m. The position of each spacecraft is specified by two values: a distance d_i in the $\hat{\boldsymbol{o}}_1$ direction, and a distance e_i in the $\hat{\boldsymbol{o}}_2$ direction. Since this formation must lie completely in one of the Hill-frame planes, the distance f_i in the $\hat{\boldsymbol{o}}_3$ direction is defined to be zero. Referring to Fig. 3.3, the positions of each spacecraft are prescribed as follows.

$$d_1 = r\cos(\theta) \qquad e_1 = r\sin(\theta) \qquad f_1 = 0 \tag{3.19a}$$

$$d_2 = r\cos(\theta + 2\pi/3) \qquad e_2 = r\sin(\theta + 2\pi/3) \qquad f_2 = 0 \tag{3.19b}$$

$$d_3 = r\cos(\theta + 4\pi/3) \qquad e_3 = r\sin(\theta + 4\pi/3) \qquad f_3 = 0 \tag{3.19c}$$

The center of mass condition is automatically satisfied by prescribing the positions of the equal-mass spacecraft to lie at the vertices of an equilateral triangle whose center coincides with the origin of the Hill frame. By evaluating the products of inertia, the formation is shown to satisfy the principal axes condition

$$I_{ef} = mr^2 \sum_{i=1}^{3} e_i f_i = 0 \tag{3.20}$$

$$I_{df} = mr^2 \sum_{i=1}^{3} d_i f_i = 0 \tag{3.21}$$

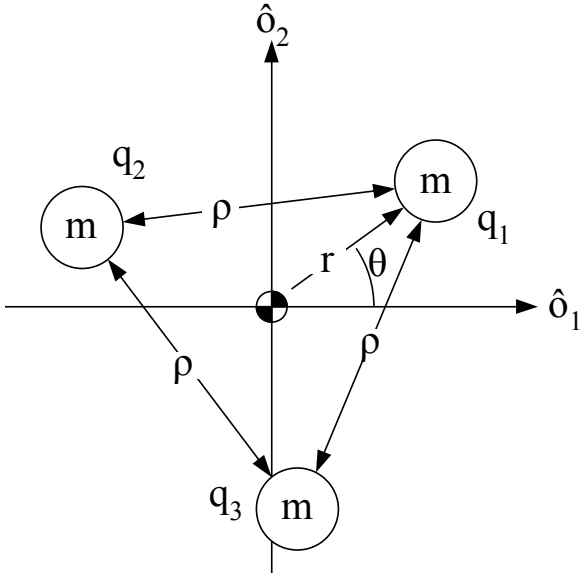

Figure 3.3: Equilateral triangle spacecraft formation.

and

$$\begin{aligned} I_{de} &= mr^2 \sum_{i=1}^{3} d_i e_i \\ &= mr^2\left(\cos\theta\sin\theta + \cos\left(\theta+\frac{2\pi}{3}\right)\sin\left(\theta+\frac{2\pi}{3}\right) + \cos\left(\theta+\frac{4\pi}{3}\right)\sin\left(\theta+\frac{4\pi}{3}\right)\right) \\ &= mr^2\left(\cos^2\theta\left(-\frac{\sqrt{3}}{4}+\frac{\sqrt{3}}{4}\right)+\sin^2\theta\left(-\frac{\sqrt{3}}{4}+\frac{\sqrt{3}}{4}\right)+\cos\theta\sin\theta\left(1+\frac{1}{4}-\frac{3}{4}+\frac{1}{4}-\frac{3}{4}\right)\right) \\ &= 0 \end{aligned} \tag{3.22}$$

As indicated previously, for a static three-spacecraft formation, which is by nature constrained to lie in one of the Hill frame planes, there are six equations that must be satisfied to ensure that the spacecraft are stationary with respect to the Hill frame. These equations of motion are linear with respect to the charge products and can be represented in matrix form as

$$m\rho^3 \begin{bmatrix} a_d d_1 \\ a_d d_2 \\ a_d d_3 \\ a_e e_1 \\ a_e e_2 \\ a_e e_3 \end{bmatrix} = \begin{bmatrix} d_1-d_2 & d_1-d_3 & 0 \\ d_2-d_1 & 0 & d_2-d_3 \\ 0 & d_3-d_1 & d_3-d_2 \\ e_1-e_2 & e_1-e_3 & 0 \\ e_2-e_1 & 0 & e_2-e_3 \\ 0 & e_3-e_1 & e_3-e_2 \end{bmatrix} \begin{bmatrix} Q_{12} \\ Q_{13} \\ Q_{23} \end{bmatrix} \tag{3.23}$$

As seen in Fig. 3.3, the inter-spacecraft distance is ρ. Using simple trigonometry, the value of ρ is found to be $\rho = 2r\cos(\pi/3) = r\sqrt{3}$.

To simplify the analysis, each position d_i and e_i is written as the product of r and a trigonometric function of θ so that $d_i = r\tilde{d}_i(\theta)$, and $e_i = r\tilde{e}_i(\theta)$. The tilde functions are defined as

$$\tilde{d}_1(\theta) = \cos(\theta) \qquad \tilde{e}_1(\theta) = \sin(\theta) \tag{3.24a}$$
$$\tilde{d}_2(\theta) = \cos(\theta + 2\pi/3) \qquad \tilde{e}_2(\theta) = \sin(\theta + 2\pi/3) \tag{3.24b}$$
$$\tilde{d}_3(\theta) = \cos(\theta + 4\pi/3) \qquad \tilde{e}_3(\theta) = \sin(\theta + 4\pi/3) \tag{3.24c}$$

This definition is convenient because r can be factored out of the differences in position so that $d_i - d_j$ becomes $r(\tilde{d}_i - \tilde{d}_j)$. In this respect, the tilde functions define a sort of unitless distance. The appropriate trigonometric identities are now employed to find the position differences between the spacecraft.

$$\tilde{d}_1 - \tilde{d}_2 = -\sqrt{3}\sin(\theta + 4\pi/3) \qquad \tilde{e}_1 - \tilde{e}_2 = \sqrt{3}\cos(\theta + 4\pi/3) \tag{3.25a}$$
$$\tilde{d}_1 - \tilde{d}_3 = \sqrt{3}\sin(\theta + 2\pi/3) \qquad \tilde{e}_1 - \tilde{e}_3 = -\sqrt{3}\cos(\theta + 2\pi/3) \tag{3.25b}$$
$$\tilde{d}_2 - \tilde{d}_3 = -\sqrt{3}\sin(\theta) \qquad \tilde{e}_2 - \tilde{e}_3 = \sqrt{3}\cos(\theta) \tag{3.25c}$$

Note the simple relationship that exists between the position differences and the positions themselves:

$$\tilde{d}_1 - \tilde{d}_2 = -\tilde{e}_3\sqrt{3} \qquad \tilde{e}_1 - \tilde{e}_2 = \tilde{d}_3\sqrt{3} \tag{3.26a}$$
$$\tilde{d}_1 - \tilde{d}_3 = \tilde{e}_2\sqrt{3} \qquad \tilde{e}_1 - \tilde{e}_3 = -\tilde{d}_2\sqrt{3} \tag{3.26b}$$
$$\tilde{d}_2 - \tilde{d}_3 = -\tilde{e}_1\sqrt{3} \qquad \tilde{e}_2 - \tilde{e}_3 = \tilde{d}_1\sqrt{3} \tag{3.26c}$$

Based upon these results, Eqn. (3.23) can be rewritten in a much simpler form for the equilateral triangle special case:

$$m\rho^2 \begin{bmatrix} a_d\tilde{d}_1 \\ a_d\tilde{d}_2 \\ a_d\tilde{d}_3 \\ a_e\tilde{e}_1 \\ a_e\tilde{e}_2 \\ a_e\tilde{e}_3 \end{bmatrix} = \begin{bmatrix} -\tilde{e}_3 & \tilde{e}_2 & 0 \\ \tilde{e}_3 & 0 & -\tilde{e}_1 \\ 0 & -\tilde{e}_2 & \tilde{e}_1 \\ \tilde{d}_3 & -\tilde{d}_2 & 0 \\ -\tilde{d}_3 & 0 & \tilde{d}_1 \\ 0 & \tilde{d}_2 & -\tilde{d}_1 \end{bmatrix} \begin{bmatrix} Q_{12} \\ Q_{13} \\ Q_{23} \end{bmatrix} \tag{3.27}$$

As discussed in the analysis of the arbitrary triangular formation, the center of mass condition eliminates two equations, one for each direction, while the principal axes condition removes one more equation. To this end, the second, fourth, and sixth equations are removed. The remaining equations, as listed in Eqn. (3.28), are used to solve for the charge products:

$$m\rho^2 \begin{bmatrix} a_d\tilde{d}_1 \\ -a_e\tilde{e}_2 \\ a_d\tilde{d}_3 \end{bmatrix} = \begin{bmatrix} -\tilde{e}_3 & \tilde{e}_2 & 0 \\ \tilde{d}_3 & 0 & -\tilde{d}_1 \\ 0 & -\tilde{e}_2 & \tilde{e}_1 \end{bmatrix} \begin{bmatrix} Q_{12} \\ Q_{13} \\ Q_{23} \end{bmatrix} \tag{3.28}$$

Solving for the charge products yields

$$\begin{bmatrix} Q_{12} \\ Q_{13} \\ Q_{23} \end{bmatrix} = \frac{-m\rho^2}{\tilde{d}_1\tilde{e}_2\tilde{e}_3 - \tilde{e}_1\tilde{e}_2\tilde{d}_3} \begin{bmatrix} \tilde{d}_1\tilde{e}_2 & \tilde{e}_1\tilde{e}_2 & \tilde{d}_1\tilde{e}_2 \\ \tilde{e}_1\tilde{d}_3 & \tilde{e}_1\tilde{e}_3 & \tilde{d}_1\tilde{e}_3 \\ \tilde{e}_2\tilde{d}_3 & \tilde{e}_2\tilde{e}_3 & \tilde{e}_2\tilde{d}_3 \end{bmatrix} \begin{bmatrix} a_d\tilde{d}_1 \\ -a_e\tilde{e}_2 \\ a_d\tilde{d}_3 \end{bmatrix} \tag{3.29}$$

Since the unknown charge products are on the left side of the equation, all that is left is to bring the solutions for the charge products to their simplest forms. For this task the third equation is examined. After substituting Eqn. (3.24) into Eqn. (3.29), multiplying, and using double and triple angle identities, the value of the charge product, Q_{23} is represented in the surprisingly simple form of a sinusoidal function of 2θ with an amplitude and offset that are both functions of a_d and a_e:

$$Q_{23} = m\rho^2 \left(a_e - a_d\right) \frac{\sqrt{3}}{3} \cos\left(2\theta\right) + m\rho^2 \left(a_e + a_d\right) \frac{\sqrt{3}}{6} \tag{3.30}$$

A similar approach can be taken to find Q_{12} and Q_{13}, however it is easier to recognize that each spacecraft is offset by 120°, and since the spacecraft are identical, the solutions for the charge products will only differ in phase angle.

$$Q_{12} = m\rho^2 \left(a_e - a_d\right) \frac{\sqrt{3}}{3} \cos\left(2\theta + \frac{2\pi}{3}\right) + m\rho^2 \left(a_e + a_d\right) \frac{\sqrt{3}}{6} \tag{3.31}$$

$$Q_{13} = m\rho^2 \left(a_e - a_d\right) \frac{\sqrt{3}}{3} \cos\left(2\theta - \frac{2\pi}{3}\right) + m\rho^2 \left(a_e + a_d\right) \frac{\sqrt{3}}{6} \tag{3.32}$$

These solutions are displayed in Fig. 3.4. The subfigures each show solutions in which the triangle formation lies in a different Hill frame plane. Compared to the analytical equilateral triangle solutions in References 1 and 4, these results are more general because they are valid for arbitrary formation orientation, θ, and alignment with any of the Hill frame planes.

According to Reference 1, sparse aperture interferometry requires that an array of sensors be distributed around a planar circle. Although the static equilateral triangle formation is one of the simplest such formations, it could serve as a technological building block toward more complex formations. Such formations may include circular formations of large numbers of spacecraft or dynamic equilateral triangle formations that are capable of changing both size and orientation.

Again, although charge products, Q_{ij}, can always be determined, it may be impossible to find constant charges, $\tilde{q}_i$, necessary to physically implement a formation. As an example, refer to Fig. 3.4. The sub-figures display the charge products necessary to maintain a static equilateral triangle formation for any given orientation in the $\hat{\boldsymbol{o}}_r - \hat{\boldsymbol{o}}_\theta$, $\hat{\boldsymbol{o}}_r - \hat{\boldsymbol{o}}_h$, and $\hat{\boldsymbol{o}}_\theta - \hat{\boldsymbol{o}}_h$ planes. The gray areas in the sub-figures indicate orientations that are physically unimplementable. From Fig. 3.4(a) it can be seen that a static equilateral triangle formation can be implemented with any orientation in the $\hat{\boldsymbol{o}}_r - \hat{\boldsymbol{o}}_\theta$ plane. Unfortunately the $\hat{\boldsymbol{o}}_r - \hat{\boldsymbol{o}}_h$

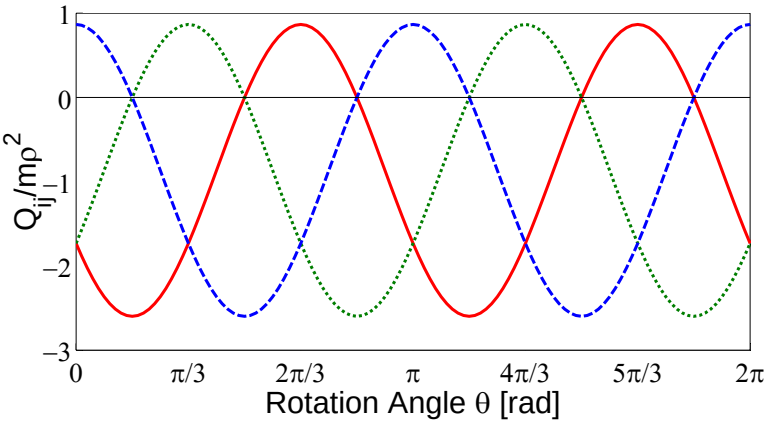

(a) $\hat{\boldsymbol{o}}_1 = \hat{\boldsymbol{o}}_r$ and $\hat{\boldsymbol{o}}_2 = \hat{\boldsymbol{o}}_\theta$ therefore $a_d = -3$ and $a_e = 0$

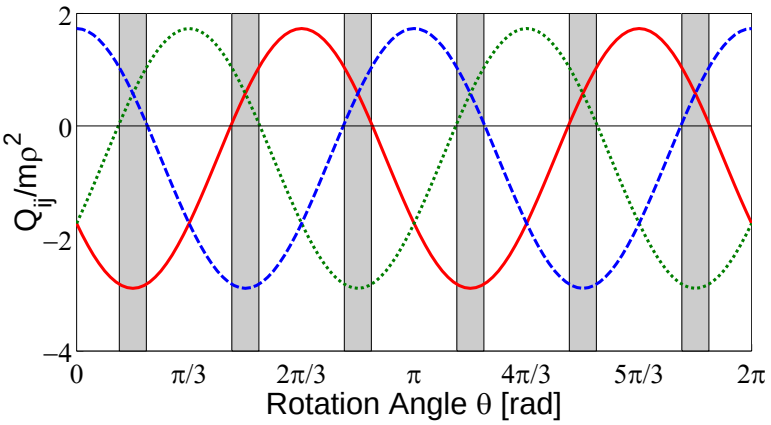

(b) $\hat{\boldsymbol{o}}_1 = \hat{\boldsymbol{o}}_r$ and $\hat{\boldsymbol{o}}_2 = \hat{\boldsymbol{o}}_h$ therefore $a_d = -3$ and $a_e = 1$

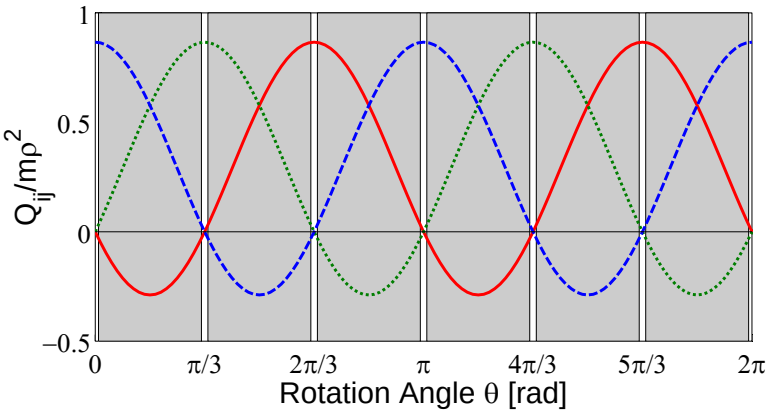

(c) $\hat{\boldsymbol{o}}_1 = \hat{\boldsymbol{o}}_\theta$ and $\hat{\boldsymbol{o}}_2 = \hat{\boldsymbol{o}}_h$ therefore $a_d = 0$ and $a_e = 1$

Figure 3.4: Q_{ij} for equilateral triangular formation aligned with different Hill frame planes. Q_{12} is — , Q_{13} is · · · ,Q_{23} is - - - .

plane and $\hat{\boldsymbol{o}}_\theta - \hat{\boldsymbol{o}}_h$ plane formations do not share this quality. In the $\hat{\boldsymbol{o}}_r - \hat{\boldsymbol{o}}_h$ plane, the equilateral triangle can only be implemented in certain ranges of θ. By a visual inspection of the charge products in Fig. 3.4(b) it can be seen that neither of the conditions outlined at the end of Sect. 3.2 are met in the shaded areas – either one charge product is zero or one charge product is negative. By inserting the appropriate values for a_d and a_e into the equations for the charge products and solving for the roots, the ranges where a static formation is possible are found to be $-\phi + \frac{m\pi}{3} < \theta < \phi + \frac{m\pi}{3}$ where m is an integer and $\phi = \arctan\left(\sqrt{3}\left(-2+\sqrt{5}\right)\right)$. For the equilateral triangle formation in the $\hat{\boldsymbol{o}}_\theta - \hat{\boldsymbol{o}}_h$ plane, static formations are only possible at discrete values of θ where $\theta = m\pi/3$. This corresponds to equilateral triangle formations where one of the spacecraft lie either on the $\hat{\boldsymbol{o}}_\theta$ axis or the $\hat{\boldsymbol{o}}_h$ axis. The reason that this formation is only possible at such singular points is because at all other values of θ, one of the charge products is negative, violating the first condition of Sect. 3.2. At the values of θ where the formation can be implemented, one of the charge products is moving from positive to negative while another charge product is moving from negative to positive. Only at these points is the product $Q_{12}Q_{23}Q_{13}$ non-negative, satisfying the first condition, and only at these points are two of the charge products zero, satisfying the second condition. The implications of such a situation upon control and stability have yet to be investigated.

3.4 Arbitrary N-craft formations

In the previous section, an closed-form analysis is presented for an arbitrary three-craft formation that inhabits two-dimensional space – a plane. The same arguments can be used to analyze an arbitrary N-craft formation that inhabits D-dimensional space, such as linear formations, $D = 1$, planar formations, $D = 2$, or full three-dimensional formations, $D = 3$. In this D-dimensional generalization, the number of equations that must be satisfied is $E = DN$, one equation for each craft for each direction. In a similar manner as described in the previous section, the number of static equations for an N-craft D-dimensional formation is reduced through the enforcement of the center of mass constraints and principal axes constraints. For a D-dimensional formation there are D center of mass constraints, C_{CM}, one for each dimension. For this same formation, there are $(D^2 - D)/2$ principal axes constraints, C_{PA}, one for each product of inertia for the D-dimensional formation. After applying the constraint equations, the remaining number of equations that must be satisfied to ensure a static formation is defined as the original number of equations minus the number of constraint equations. The final number of equations is denoted as $\mathcal{E}$:

$$\begin{aligned}\mathcal{E} =& E - C_{\text{CM}} - C_{\text{PA}} \\ =& DN - D - \frac{D^2 - D}{2} \\ =& DN - \frac{D^2 + D}{2}\end{aligned} \tag{3.33}$$

Therefore, for a three-dimensional formation, $\mathcal{E} = 3N-6$, for a planar formation, $\mathcal{E} = 2N-3$, and for a linear formation, $\mathcal{E} = N-1$. These results are summarized in Table 3.1.

Table 3.1: Effect of enforcing center of mass and principal axes constraints.

No. of dimensions	No. of equations before enforcing constraints	No. of equations satisfied by		No. of equations after enforcing constraints
		center of mass	principal axes	
1	N	1	0	$N-1$
2	$2N$	2	1	$2N-3$
3	$3N$	3	3	$3N-6$
D	DN	D	$\frac{D^2-D}{2}$	$DN-\frac{D^2+D}{2}$

3.4.1 Comparison of the Number of Static Equations and the Number of Charge Products

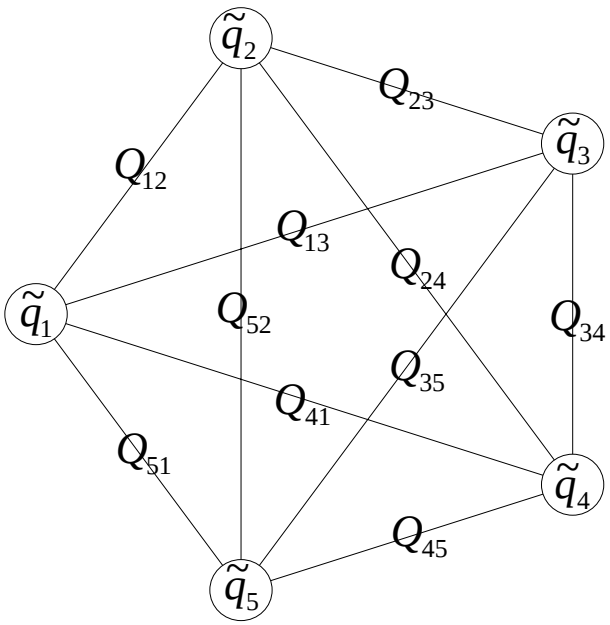

Figure 3.5: Graphical representation of the relationship between charges and charge products.

Now attention is turned to the solution of the static equations represented in Eqn. (2.3). Notice that all of these equations are linear in the charge products, Q_{ij}, so that it should be possible to solve for them using basic concepts of linear algebra. However, the number of

charge products for a given formation is typically greater than the number of static equations and under such circumstances there are infinitely many solutions for the charge products, Q_{ij}. It is therefore beneficial to make a comparison of the number of charge products versus the number of static equations for a given formation. The number of charge products for a formation, represented $\mathcal{Q}$, can be inferred from the graph displayed in Fig. 3.5. The nodes of the graph represent the charges, $\tilde{q}_i$, and the edges that connect the nodes represent the charge products, Q_{ij}. Since every node of the graph is connected to every other node, the graph is complete, and the number of edges is

$$\mathcal{Q} = \binom{N}{2} = N(N-1)/2 \tag{3.34}$$

where $\binom{N}{k}$ is a binomial coefficient.[22] Table. 3.2 compares the number of equations, $\mathcal{E}$, and number of charge products, $\mathcal{Q}$, given a certain number of spacecraft N and the number of dimensions they inhabit D. As can be seen from the table, whenever $N < D + 1$, the formation cannot exist. For example, it is impossible to construct a planar formation with only two spacecraft. Whenever $N = D + 1$ then $\mathcal{Q} = \mathcal{E}$. In this case, the linear system of equations can be solved for a unique set of charge products. Whenever $N > D + 1$ then $\mathcal{Q} > \mathcal{E}$. In this most common case, there are infinitely many possible sets of charge products that satisfy the static equations. Therefore the charge products have sufficient freedom to be optimized or minimized subject to further constraints. However, one must remember that a constant charge formation is implemented by the charges $\tilde{q}_i$ rather than the charge products. As will be shown in Sect. 3.4.2, the charge products that satisfy the static equations may lead to imaginary, or even self contradictory charge values.

Table 3.2: Comparison of number of equations with number of charge products for several values of N and D.

No.	No. of Dimensions				$\mathcal{Q}$
Crafts	1	2	3	D	No. Q_{ij}s
2	1	-	-	$\frac{D-D^2}{2}$	1
3	2	3	-	$\frac{3D-D^2}{2}$	3
4	3	5	6	$\frac{5D-D^2}{2}$	6
5	4	7	9	$\frac{7D-D^2}{2}$	10
6	5	9	12	$\frac{9D-D^2}{2}$	15
N	$N-1$	$2N-3$	$3N-6$	$\frac{(2N-1)D-D^2}{2}$	$\frac{N(N-1)}{2}$
	$\mathcal{E}$ No. of Equations				

3.4.2 Relationship Between Charge Products and Charges

Since constant-charge static Coulomb formations will ultimately be implemented with the charges q_i rather than the charge products Q_{ij}, it is important to completely understand the

relationship that exists between the charges and charge products. For the simple case of two spacecraft, there is one charge product and two charges. There can therefore be infinitely many charge solutions of the form $\tilde{q}_1 = Q_{12}/\tilde{q}_2$ where $\tilde{q}_2$ can be arbitrarily chosen. For the case of a three-spacecraft triangular formation, there are three charge products and three charges. A solution can always be found for these charges from the charge products, however, these charge products may be imaginary and therefore unimplementable. (This is discussed in detail in Section 3.2 with examples in the latter part of Section 3.3.) For cases of formations with more than three spacecraft, the situation becomes even more complicated. As seen in Table. 3.2, the charge products outnumber the charges so that in general, the charges cannot be uniquely determined from the charge products. Further in this section a method is introduced that may be helpful in overcoming this obstacle – pulse width modulation. However, in the meantime, the relationship between the charge products and charges is further explored.

Recall that $Q_{ij} = \tilde{q}_i\tilde{q}_j$, therefore $\tilde{q}_1 = Q_{12}/\tilde{q}_2$. From Fig. 3.5, the latter equation corresponds to moving from $\tilde{q}_1$ through Q_{12} to $\tilde{q}_2$. Similarly, starting at $\tilde{q}_2$ and moving to $\tilde{q}_3$ yields $\tilde{q}_2 = Q_{23}/\tilde{q}_3$, and starting at $\tilde{q}_3$ and moving to $\tilde{q}_1$ yields $\tilde{q}_3 = Q_{31}/\tilde{q}_1$. Combining these three equations yields

$$\tilde{q}_1^2 = \frac{Q_{12}Q_{31}}{Q_{23}} \tag{3.35}$$

This equation corresponds to a path that starts at $\tilde{q}_1$ and moves through $\tilde{q}_2$ and $\tilde{q}_3$ and then stops at $\tilde{q}_1$. Notice that the Q_{ij} crossed during the odd steps, (e.g. Q_{12} and Q_{31}), are in the numerator while the Q_{ij} crossed during the even steps, (e.g. Q_{23}), are in the denominator. This pattern holds for any path through the graph. The equation formed by this first loop, Eqn. (3.35), represents one condition that q_1 must satisfy. By taking alternate paths through the graph, more conditions can be found as enumerated in Table 3.3.

Table 3.3: Enumeration of loop equations for $\tilde{q}_1$.

Eqn. No	Path	Loop Equation
1	$\tilde{q}_1 - \tilde{q}_2 - \tilde{q}_3 - \tilde{q}_1$	$\tilde{q}_1^2 = \frac{Q_{12}Q_{31}}{Q_{23}}$
2	$\tilde{q}_1 - \tilde{q}_2 - \tilde{q}_4 - \tilde{q}_1$	$\tilde{q}_1^2 = \frac{Q_{12}Q_{41}}{Q_{24}}$
3	$\tilde{q}_1 - \tilde{q}_2 - \tilde{q}_5 - \tilde{q}_1$	$\tilde{q}_1^2 = \frac{Q_{12}Q_{51}}{Q_{25}}$
4	$\tilde{q}_1 - \tilde{q}_3 - \tilde{q}_4 - \tilde{q}_1$	$\tilde{q}_1^2 = \frac{Q_{13}Q_{41}}{Q_{34}}$
5	$\tilde{q}_1 - \tilde{q}_3 - \tilde{q}_5 - \tilde{q}_1$	$\tilde{q}_1^2 = \frac{Q_{13}Q_{51}}{Q_{35}}$
6	$\tilde{q}_1 - \tilde{q}_4 - \tilde{q}_5 - \tilde{q}_1$	$\tilde{q}_1^2 = \frac{Q_{14}Q_{51}}{Q_{45}}$

At this point, one might conclude that besides the triangular loops listed in Table 3.3, there might be many more loops leading to more and more equations that q_1 must satisfy. However, this is not the case. For instance, the path around the outside of the pentagon, starting from $\tilde{q}_1$, moving through $\tilde{q}_2$, $\tilde{q}_3$, $\tilde{q}_4$, and $\tilde{q}_5$, and then stopping again at $\tilde{q}_1$,

would produce the equation $\tilde{q}_1^2 = (Q_{12}Q_{34}Q_{51}) / (Q_{23}Q_{45})$. This equation is automatically satisfied by multiplying the first and sixth equations from Table 3.3 and then dividing by the fourth equation. In a similar manner, any loop that traverses more than three edges can be shown to be equivalent to loops that only cross three edges. For this reason, the number of equations that a charge must satisfy is equal to the number of unique triangular loops that pass through the charge's node. From Fig. 3.5, it is apparent that the number of equations $\tilde{q}_1$ must satisfy is equal to $\binom{N-1}{2} = (N-1)(N-2)/2$; i.e. the number of possible combinations of two nodes chosen from the set of all nodes except for $\tilde{q}_1$. Therefore, in order to have an implementable formation, the charge of each spacecraft, q_i, must satisfy $(N-1)(N-2)/2$ equations. If these equations are contradictory to one another, as may be the case, then there is no way to physically implement the formation with constant charges. In the event that the equations are not self contradictory, they still must satisfy the criteria outlined at the end of Sect. 3.2 to ensure that the charges are finite and real valued. Based on this it may seem impossible to find a formation that can be implemented with constant charges, however, this is not the case. As is shown in the next chapter, formations have been numerically determined for as many as nine spacecraft. However, the geometry and mass distribution necessary for a formation to be implementable are not obvious. Indeed, feasible formation geometries and mass distributions seem to be a small subset of all possible geometries and mass distributions. Perhaps the previous analysis will give insight into analytically determining families of geometries and mass distributions that lead to formations implementable by constant charge.

Formations need not be implemented only with constant charges. Pulse width modulation is a promising prospective method for controlling Coulomb formations and for overcoming the issues inherent with constant charge implementations. Roughly, pulse-width modulation is a method by which the charges of individual spacecraft are rapidly raised and lowered, or *pulsed*, such that the effective charge product between any two spacecraft is the charge product necessary to maintain a stationary formation in the Hill frame. As an example of the utility of pulse-width modulation, again consider the case of an equilateral triangle formation in the $\hat{\boldsymbol{o}}_\theta - \hat{\boldsymbol{o}}_h$ plane. As seen in Fig. 3.4(c), to attain an orientation of $\theta = \pi/6$, the formation must contain two positive charge products and one negative charge product. Since $\tilde{q}_i = \sqrt{Q_{ij}Q_{ik}/Q_{jk}}$, this set of charge products would only be possible with complex-valued charges. However, with pulse-width modulation, it is possible to momentarily turn a spacecraft off, (i.e. remove all charge), while charging the other two spacecraft to the appropriate charge product. By quickly cycling through all of the spacecraft in this manner, it is possible to effectively give any two spacecraft the appropriate charge product. However, rapidly changing the electrostatic potentials of the spacecraft raises technical challenges in implementing Coulomb propulsion that must eventually be addressed.

If pulse-width modulation is determined to be feasible, then an entire new realm of possibilities will be opened for stationary formations. As stated earlier, for the general 3-D, N-spacecraft formation, there are $3N-6$ equations that must be satisfied by $N(N-1)/2$ charge products. Therefore, with larger numbers of spacecraft, the number of variables avail-

able to satisfy the equations greatly outnumber the equations to be satisfied. Unfortunately, for larger numbers of spacecraft, it may become impossible to pulse fast enough to create effective charge products necessary to keep the formation stationary. Nevertheless pulse-width modulation deserves attention in future research.

The analysis of this chapter presents the closed-form solution for the following formations: all two-craft formations, linear three-craft formations, and equal-mass equilateral triangular formations. Although any two-craft and any linear three-craft formation is implementable, there are cases when the equilateral triangular formation can not be implemented. Such cases are thoroughly discussed. Further in the analysis, closed-form charge product solutions are presented for the arbitrary case of N-craft formations that satisfy center of mass and principal axes conditions. Although it is always possible to determine charge products for a given formation, these charge products may lead to imaginary or even multivalued craft charges which can not be implemented. In the following chapter, several numerical solutions for Coulomb formations are discussed.

Chapter 4

Numerical Analysis

In research, developed theory is meaningless unless it can be verified by experimentation and numerical results. This chapter details a numerical analysis of static Coulomb formations. First, the methods of analysis are described. This analysis employs a genetic algorithm to determine formations of Coulomb spacecraft for which the craft accelerations are sufficiently small so as to be considered stationary with respect to the Hill frame. Use of the genetic algorithm as an optimization tool has been growing in popularity. In the field of astrodynamics, the genetic algorithm has been applied to such objectives as the design of optimal satellite constellations,[13] the design of low-thrust trajectories,[14–16] and optimal orbital rendezvous.[17] While more traditional, gradient-based methods are efficient at handling a wide range of optimization problems, they become less useful when the cost function has a complex topography including such obstacles as discontinuities and numerous non-optimal local minima. Since the topography of the cost functions considered for the problem of determining static Coulomb formations are complex, the genetic algorithm is well applicable for this analysis. After the methods used are described, numerical results are presented. These results, including formations of two- to nine-spacecraft, serve to substantiate the analysis provided in Chapter 3 as well as to provide additional insight into formation geometries that are possible with more than three spacecraft. The final section of this chapter presents a method by which the center of mass and principal axes conditions can be used to eliminate several parameters from the search space, and thereby dramatically increase the efficiency of the genetic algorithm.

4.1 Genetic Algorithm

There are several variations of the genetic algorithm. This section outlines important aspects of the genetic algorithm used during this research. Discussion in the first subsection includes the mating, mutation, and constraint functions and the role they play in artificially evolving

solutions to the problem posed. The second subsection describes in detail the cost function used in this study, including convergence to trivial formation solutions and the course of action taken to correct this problem.

4.1.1 Basic Implementation

Let $J(\boldsymbol{p})$ represent a cost function that is to be minimized with respect to a set of parameters $\boldsymbol{p}$. Traditional gradient-based numerical optimization schemes use an initial guess for $\boldsymbol{p}$, and then proceed in the direction of steepest decent $\partial J/\partial \boldsymbol{p}$ until finally coming to rest at a local minimum. For many problems this method is sufficient, however there are certain optimization problems, such as the ones considered in this analysis, for which there are few obvious initial guesses for $\boldsymbol{p}$. Furthermore, for a cost function with a more "rugged" topography, a gradient-based optimization is likely to get trapped at a non-optimal local minimum. In the worst case scenario, a gradient-based optimization may even be unable to determine an effective direction to move due to discontinuities in the cost function $J(\boldsymbol{p})$. Genetic algorithms (GAs) are a relatively new group of methods that, at the expense of greater computational intensity, are able to overcome much of the problems of gradient-based approaches. Rather than moving downslope from an initial guess $\boldsymbol{p}_o$, the GA attempts to "evolve" an optimal solution by emulating the process of natural evolution.

There are many different forms of the genetic algorithm, however the basic form of the GA employed for this analysis is outlined in Fig. 4.1. The algorithm first creates an initial population of several non-optimal, but valid, parameter sets $\boldsymbol{p}$. The cost function $J(\boldsymbol{p})$ is evaluated for each set of parameters and the members of the population are then sorted from most "fit" to least "fit." The members of the population that are least fit to survive are then eliminated while the fittest members are allowed to mate with one another in order to recombine their traits and pass them on to future generations. The offspring that result from this mating process take the place of the weaker members of the population. At this point, a portion of the offspring undergo an additional mutation of their parameters. The purpose of mutation is to ensure that portions of the search space may be reached that might not otherwise be reached through the process of mating. The severity of mutation and the number of members who are mutated are both parameters of the algorithm itself which may be tuned in order to improve the performance of the GA. After the process of mating and mutating, some of the new parameter sets $\boldsymbol{p}$ may be found to lie outside of bounds for a reasonable parameter set. If this is so, then the parameters that are located outside of bounds are replaced with values that are within reasonable bounds. Once all of the new members have been constrained in this manner, their fitness is evaluated through $J(\boldsymbol{p})$ and they are sorted back into the general population. At this point the process begins again. With each generation, the fitness of the population improves until either the population converges to a solution, or the maximum number of generations has been exceeded.

In earlier versions of the genetic algorithm, and even many contemporary versions,

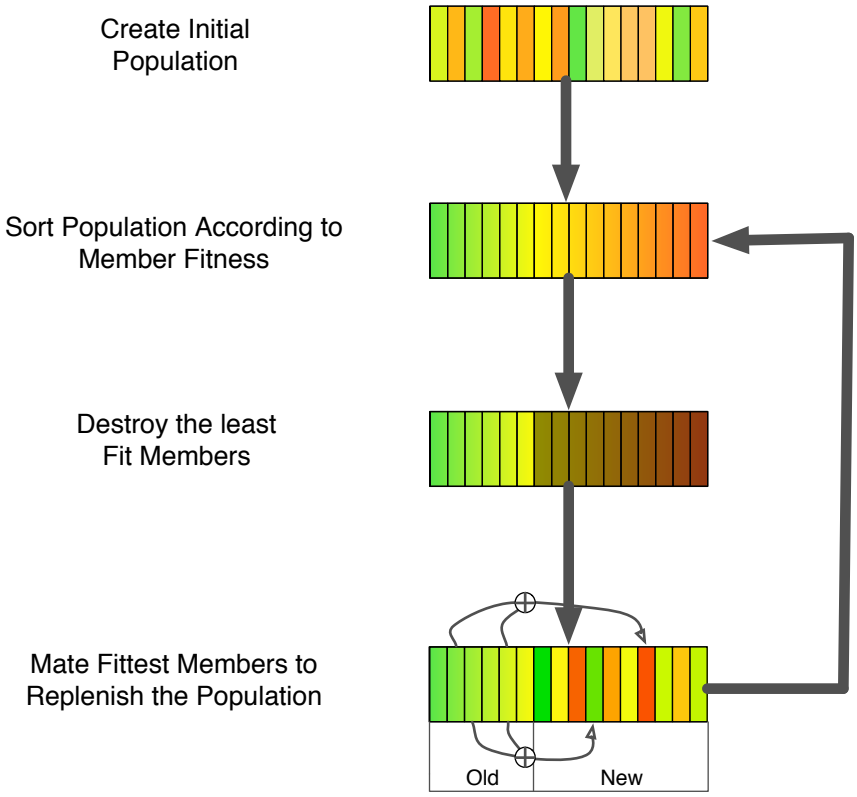

Figure 4.1: Illustration of the single-processor genetic algorithm.

parameters are represented in binary form and then concatenated into a single string. The appeal of this method is that the "genome" of the members – strings of ones and zeros – more closely resemble the genetic representations found in nature – strands of DNA. Then, following the analogy of nature, the mating process can be represented by a string operation in which the child inherits portions of the father's string, and portions of the mother's string. Rather than use this method for representing a set of parameters, the implementation of the GA used in this research maintains each parameter as a separate and independent entity represented in computer memory as a double precision value. The rationale for this choice is that in experiments done with several different implementations of the genetic algorithm, the methods involving binary string concatenation of parameters are incapable of exploring the search space as efficiently as methods in which the parameters were kept independent. In addition, there is considerable programming and computational overhead in translating the parameters to and from the binary strings. The remainder of this section describes in more detail the basic methods of mating, mutation, and constraint used for this research.

In the GA implementation used in this research, the process of mating is accomplished by applying a set of weights, $\boldsymbol{w}$ to the parents so that the offspring represents a weighted

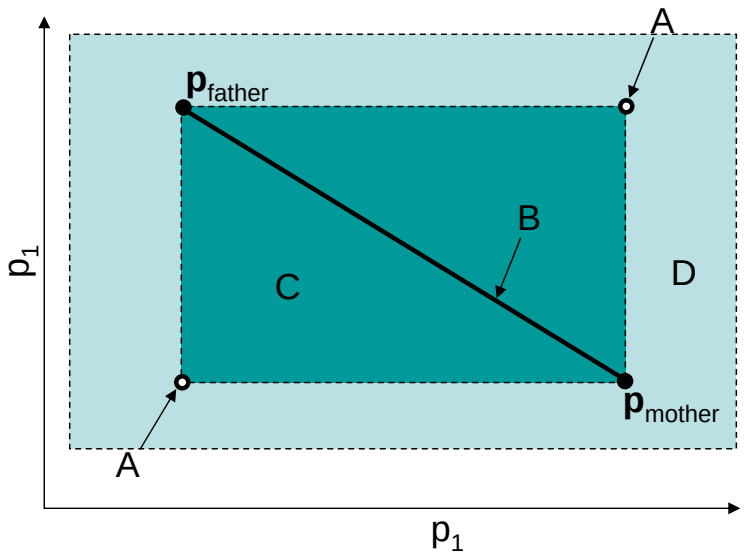

	Allowable Values of w_i	Resulting Offspring
A	$w_i = 0$ or 1	Offspring are a recombination of the parameters of the parents
B	$w_i = W$ for all i where $0 < W < 1$	Offspring appear at any point on the line connecting the parents
C	$0 < w_i < 1$	Offspring appear at any point in n dimensional cuboid bounded by parent's parameters
D	$-0.25 < w_i < 1.25$	Same as C except that boundaries of cuboid are expanded by 25%

Figure 4.2: Various methods of parameter mating.

average of the parents. This method of mating is represented algebraically as follows.

$$p_{i_{\text{offspring}}} = w_i p_{i_{\text{father}}} + (1 - w_i)\, p_{i_{\text{mother}}} \tag{4.1}$$

By limiting the values that $\boldsymbol{w}$ is allowed to have, different effects can be achieved. Figure 4.2, (and the associated table), enumerates several different methods considered during the course of this research. However the final method chosen for mating is a combination of methods A and D. Half of the time, the parameters of the offspring are a simple recombination of the parameters of the parents, (method A). The other half of the time, the parameters of the offspring are an interpolation between or an extrapolation from the parent parameters, (method D).

Parameter mutation is included to increase variability and explore new portions of the parameter space. Mutation is performed by simply adding a randomly generated value R to

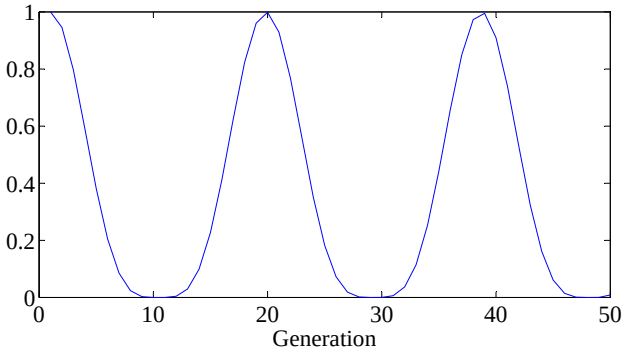

Figure 4.3: Plot of generation-dependent mutation scaling function $\gamma(g)$.

the offspring's current parameter value:

$$\bar{p}_i = p_i + R \tag{4.2}$$

where $\bar{p}_i$ is the value of the parameter after mutation and R is a random number of Gaussian distribution that has been scaled as follows.

$$R = r_{\text{norm}} \left(p_{i\text{max}} - p_{i\text{min}} \right) \gamma \left(g \right) \tag{4.3}$$

The value r_{norm} is a random number of Gausian distribution with a mean of zero, variance of one and a standard deviation of one. The values $p_{i\text{max}}$ and $p_{i\text{min}}$ are the maximum and minimum values that the parameter p_i can hold. Therefore the term $(p_{i\text{max}} - p_{i\text{min}})$ serves as a scaling factor so that the magnitude of the mutation is proportional the range of value that p_i can hold. Finally, $\gamma\left(g\right)$ is a scaling constant that is a function of the current generation g. The exact form of $\gamma(g)$ is

$$\gamma\left(g\right) = \frac{1}{4}\left(\cos\left(\frac{g}{3}\right) + 1\right)^2 \tag{4.4}$$

The reason for having a scaling constant that is a function of generation is so that the severity of the mutation will be different from one generation to the next. In some generations, the drastic mutations will more thoroughly explore portions of the search space that may be overlooked during the mating process, while during other generations, the mutations will serve as small perturbations that will help to converge on a solution more quickly. Eqn. (4.4) is specifically designed to be a positive periodic function of generation with a longer dwell period at values closer to zero. A plot of this function is seen in Fig. 4.3.

After the members of the population have been mated together and a portion of the offspring have been mutated, the population must be constrained so that all of the parameters are within acceptable bounds. The method used for the early stages of this research was to "fix" the illegitimate members by deleting the parameter that was outside of allowable bounds and replacing it with a value inside of the bounds. The effect of replacing illegitimate values is similar to a mutation of parameters, so that the constrained members are reasonably

related to other members of the population and will therefore be helpful in searching the parameter space.

Another method of constraint used towards the conclusion of the research not only ensures that each parameter is inside of the legal bounds, but also perturbs each of the parameter values so that the center of mass and principal axes conditions are more closely satisfied. The effect is that the search space is reduced in dimension by the enforcement of these necessary conditions. This method of parameter reduction is discussed in more detail in Sect. 4.4.

4.1.2 Establishing a Cost Function for Determining Static Coulomb Formations

For the specific application of the GA toward the determination of static Coulomb formations, let $\boldsymbol{p}$ be defined as

$$\boldsymbol{p} = (x_1, y_1, z_1, q_1, \cdots, x_N, y_N, z_N, q_N) \tag{4.5}$$

In the results presented in this thesis, the numerical search is simplified by assuming that the mass of each spacecraft is 1kg, therefore mass values need not be included in the list of parameters.

In order to numerically search for static Coulomb formations, a cost function $J(\boldsymbol{p})$ is defined to be a positive definite measure of the spacecraft accelerations in the Hill frame. As the accelerations of the spacecraft decrease, $J(\boldsymbol{p})$ also decreases. In the limiting case, $J(\boldsymbol{p})$ is identically zero. The following discussion explores several cost functions and strategies used during the course of this research. First, terms used in the cost function must be clearly defined. Recall from Chapter 2 that the acceleration components of a spacecraft are expressed in the Hill frame as:

$$\ddot{x}_i = 3n^2 x_i + \frac{k_c}{m_i} \sum_{j=1}^{N} \frac{x_i - x_j}{\rho_{ji}^3} q_i q_j \tag{4.6a}$$

$$\ddot{y}_i = \frac{k_c}{m_i} \sum_{j=1}^{N} \frac{y_i - y_j}{\rho_{ji}^3} q_i q_j \tag{4.6b}$$

$$\ddot{z}_i = -n^2 z_i + \frac{k_c}{m_i} \sum_{j=1}^{N} \frac{z_i - z_j}{\rho_{ji}^3} q_i q_j \tag{4.6c}$$

As stated previously, velocities do not appear in these equations because they can be prescribed as zero. The acceleration of spacecraft i is expressed in vector notation as

$$\ddot{\boldsymbol{\rho}}_i = {}^{\mathcal{H}}\begin{bmatrix} \ddot{x}_i \\ \ddot{y}_i \\ \ddot{z}_i \end{bmatrix} \tag{4.7}$$

In addition, the acceleration imparted to spacecraft i by its electrostatic interaction with spacecraft j is represented by $\ddot{\boldsymbol{\rho}}_{ij}$:

$$\ddot{\boldsymbol{\rho}}_{ij} = \frac{1}{m_i} \frac{\boldsymbol{\rho}_i - \boldsymbol{\rho}_j}{|\boldsymbol{\rho}_i - \boldsymbol{\rho}_j|^3} q_i q_j \tag{4.8}$$

Finally, if the Hill frame accelerations are represented by $\ddot{\boldsymbol{\rho}}_{\mathcal{H}i} = \begin{bmatrix} 3x_i & 0 & -z_i \end{bmatrix}^T$ then Eqn. (4.6) can be represented compactly as

$$\ddot{\boldsymbol{\rho}}_i = \ddot{\boldsymbol{\rho}}_{\mathcal{H}i} + \sum_{j=1}^{N} \ddot{\boldsymbol{\rho}}_{ij} \tag{4.9}$$

The first cost function considered during the research is simply a sum of the magnitudes of the spacecraft accelerations:

$$J(\boldsymbol{p}) = \sum_{i=1}^{N} \|\ddot{\boldsymbol{\rho}}_i\| \tag{4.10}$$

Since the goal is to eliminate all spacecraft acceleration, Eqn. (4.10) is the most obvious choice for a cost function. Unfortunately, there is a fundamental flaw with this cost function that hinders it from being useful. While using this cost function, the GA is always drawn toward a trivial solution in which the charges on all but one of the craft go to zero, and the spacecraft align themselves with the $\hat{\boldsymbol{o}}_\theta$ axis. In this situation there are no inter-craft forces and since the spacecraft lie in the same circular orbit, there are no accelerations in the Hill frame. So even though the static requirements are perfectly satisfied, the resulting formation takes no advantage of Coulomb interaction.

In an initial effort to avoid this trivial solution, areas in the parameter space near the trivial solution were quarantined. If a charge decreased below a certain acceptable level, the constraint function would reassign the charge to a more acceptable level. Unfortunately, this method does not improve the situation. Instead of reaching the trivial solution, the population converges to a non-optimal solution somewhere along the constraint boundary.

To remedy the problem, a weighting term is introduced. Once included in the cost function, the additional terms allow the algorithm to converge to a non-trivial solution. This weighting term is the inverse of the sum of the magnitudes of the inter-spacecraft accelerations, $\ddot{\boldsymbol{\rho}}_{ij}$. With the new weighting term, the cost function is

$$J(\boldsymbol{p}) = \sum_{i=1}^{N} \|\ddot{\boldsymbol{\rho}}_i\| \Bigg/ \sum_{j=1}^{N} \sum_{i=1}^{N} \|\ddot{\boldsymbol{\rho}}_{ij}\| \tag{4.11}$$

Just as before, this cost function is a positive definite measure of acceleration. The additional term reflects the strength of the Coulomb interaction between the spacecraft. Formations with little Coulomb interaction – such as the trivial case described earlier – are severely

penalized, while formations that have strong Coulomb interaction are rewarded. So this new cost function actually exhibits two advantages over the former cost function. Not only does this function effectively mask the trivial solution, but it has the additional benefit of being naturally disposed toward formations with stronger Coulomb interaction.

4.2 Numerical Results for Hill Frame Formations

Figure 4.4 displays examples of various static Coulomb formations determined by using the cost function of Eqn. (4.11). The axes labeled $\hat{\boldsymbol{o}}_r$, $\hat{\boldsymbol{o}}_\theta$, and $\hat{\boldsymbol{o}}_h$ are the Hill frame axes, while the dashed lines are the principal axes of the formation. Recall from Chapter 2 that for a static formation, the principal axes of the formation must be aligned with the Hill frame axes. In the figures, however, there are instances where the principal axes do not appear to lie parallel to the Hill axes. One reason for the lack of alignment is that for axisymmetric formations, such as a linear or equilateral triangle formation, the principal axes perpendicular to the axis of symmetry are arbitrary. For formations that are not axisymmetric, the offset between the principal axes and the Hill axes may be ascribed to insufficient convergence.

The criterion for considering a formation "static" in the Hill frame is that the average acceleration magnitude of the formation spacecraft should be a small fraction of the typical Hill acceleration that a spacecraft might experience. Figure 4.4(a) displays a typical two-spacecraft formation. These simple formations might one day be useful as virtual tethers between two spacecraft. Figures 4.4(b)–4.4(e) show various Coulomb formations that are determined for three spacecraft. There are two linear formations, one aligned with the $\hat{\boldsymbol{o}}_h$ axis, Figure 4.4(b), and one aligned with the $\hat{\boldsymbol{o}}_\theta$ axis, Figure 4.4(c). These collinear three-craft static Coulomb formations have been shown to exist analytically by King and Parker.[1,2] Like the two-spacecraft formations, these formations may also be useful as virtual Coulomb tethers. However, unlike its two-craft counterpart, the sum of the magnitude of the inter-craft forces for this formation are up to seven times stronger. Figures 4.4(d) and Figure 4.4(e) display triangular formations that are perpendicular to the $\hat{\boldsymbol{o}}_\theta$ and $\hat{\boldsymbol{o}}_h$ axes respectively.

Figure 4.5 illustrates several static N-craft Coulomb formations for $N > 3$. As can be seen from these figures, the formations become increasingly more complex with each additional spacecraft. As seen in Fig.4.5(a), many of the four-craft formations are nearly planar, triangular formations. By observing the formations of Fig. 4.5, certain common characteristics are recognized for formations of five to nine spacecraft. For instance, there is a tendency toward geometric symmetry about the plane perpendicular to the $\hat{\boldsymbol{o}}_h$ axis. This tendency is clearly seen in the shadows to the right-hand side of the formations. Also, the spacecraft tend to lie closer to the $\hat{\boldsymbol{o}}_\theta - \hat{\boldsymbol{o}}_h$ plane. This tendency is most obvious for the nearly planar formations in Fig. 4.5(a), 4.5(c) and 4.5(d). As the number of spacecraft increase beyond nine, the formations begin to appear more disorganized.

Several of the numerically determined formations possess traits worth investigating. For

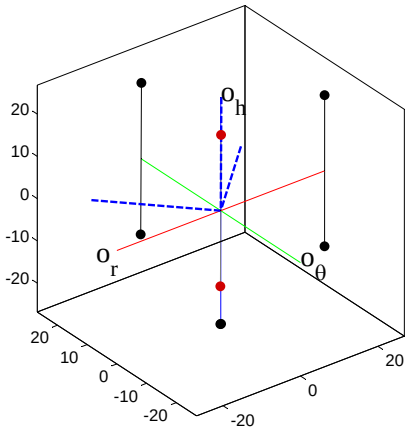

(a) Two Spacecraft Formation

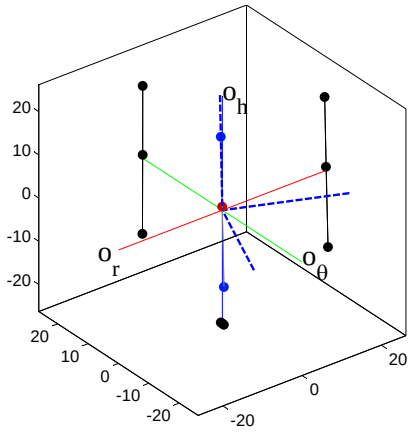

(b) $\hat{\boldsymbol{o}}_h$ Aligned Three Spacecraft Formation

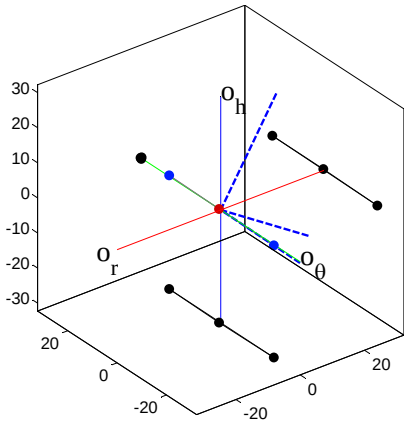

(c) $\hat{\boldsymbol{o}}_\theta$ Aligned Three Spacecraft Formation

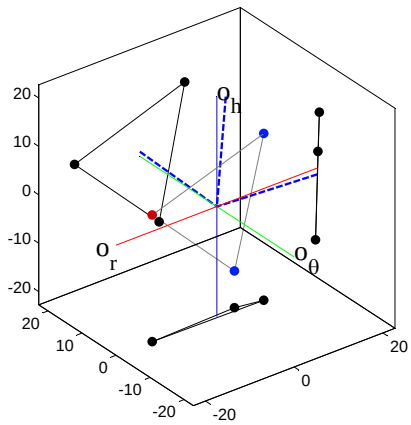

(d) $\hat{\boldsymbol{o}}_\theta$ Perpendicular Triangular Spacecraft Formation

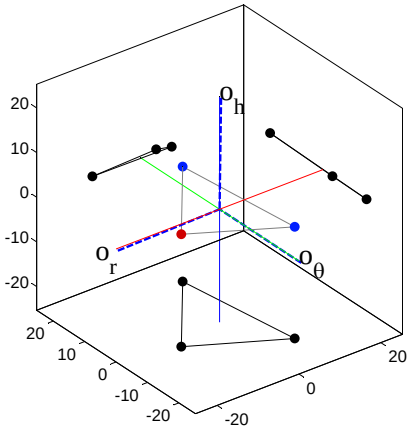

(e) $\hat{\boldsymbol{o}}_h$ Perpendicular Triangular Spacecraft Formation

Figure 4.4: Examples of two- and three-spacecraft formations determined by the GA.

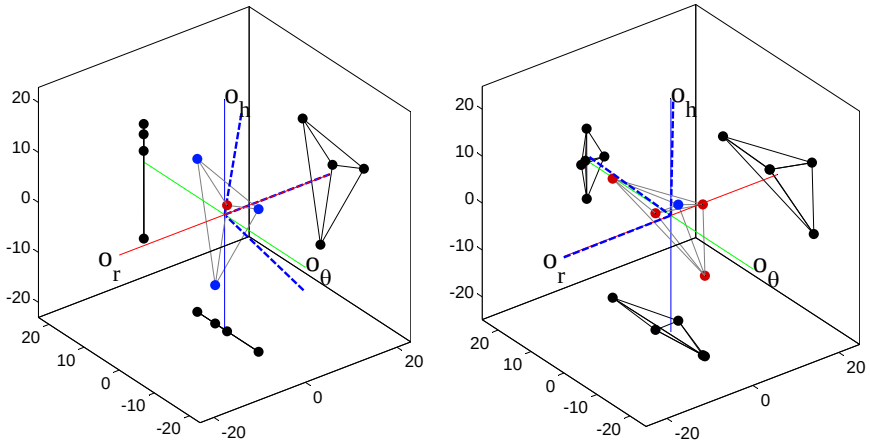

(a) Four Spacecraft Formation

(b) Five Spacecraft Formation

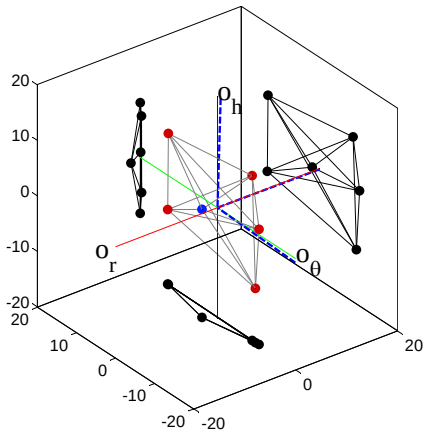

(c) Six Spacecraft Formation

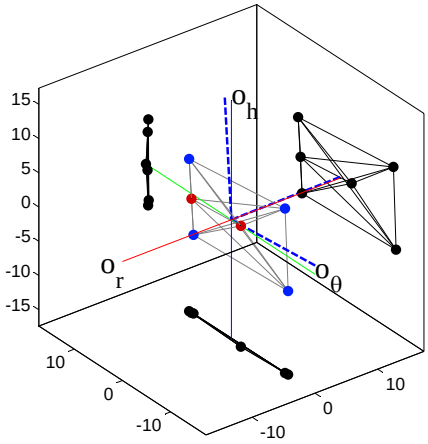

(d) Six Spacecraft Formation

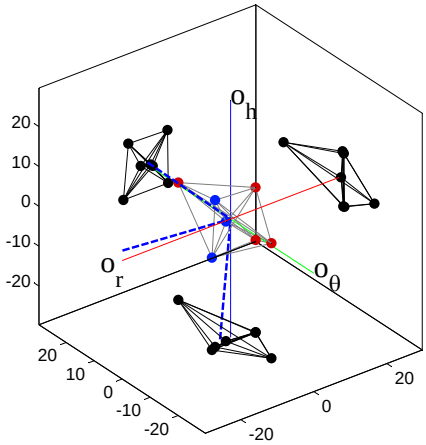

(e) Seven Spacecraft Formation

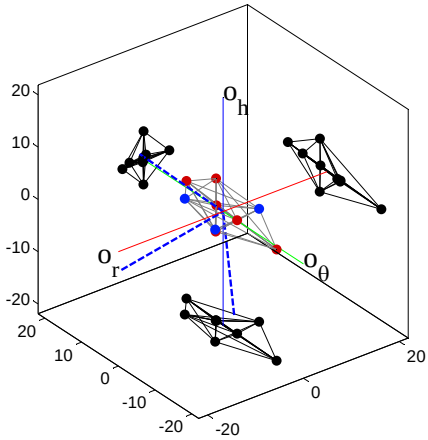

(f) Nine Spacecraft Formation

Figure 4.5: Examples of multi-spacecraft formation determined by the GA.

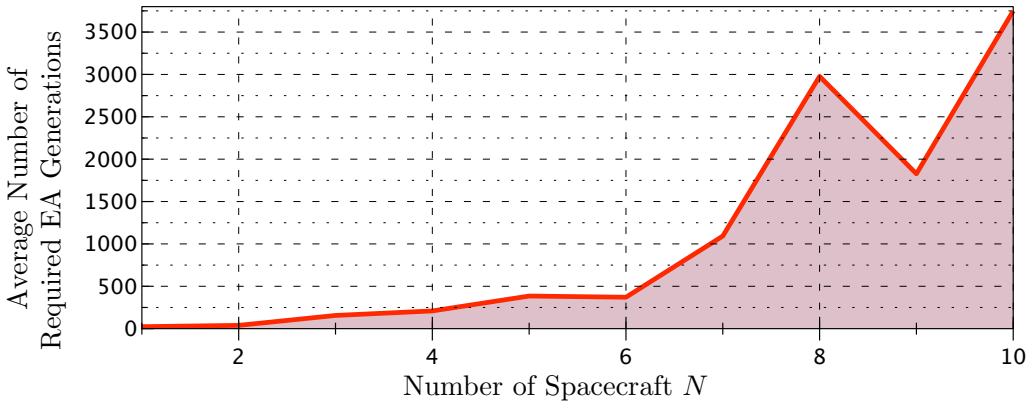

Figure 4.6: Computation necessary to realize an N-spacecraft formation using the GA

example, Fig. 4.5(c) shows a planar ring of negatively charged spacecraft with a positively charged spacecraft at a position near the center of this ring. Formations similar to this will be ideal for application in sparse aperture interferometry. The spacecraft on the circumference will have the task of collecting the signals while the craft in the center will combine them to form one high definition image. The formations represented in Fig. 4.5(e) and 4.5(b) may someday serve as virtual space structures. Such structures would have a significant weight and cost advantage over the typical truss structures in space today. Finally, all of the formations presented in this analysis attest to the variability of the formations that can be created using Coulomb charging. Unlike many formations presented in earlier results in which spacecraft lie only along the Hill frame axes or in a Hill frame plane, the results presented here indicate that freedom exists to place formation craft in many arbitrary configurations unconstrained to plane or axis.[1,2,4]

A consideration is now given to the amount of computation necessary to find an N-spacecraft formation using the genetic algorithm. Figure 4.6 displays the average number of generations necessary to find a formation with N spacecraft. The data in the figure reflects ten successful formation determinations for formations ranging from two to ten craft. As seen in the figure, the computational effort grows exponentially with the number of spacecraft included in a formation. If formations are to be determined for larger numbers of spacecraft, then computational power must be greatly increased before a numerical analysis will be possible. Additionally, there is an unexpected decrease in the computational effort required for nine spacecraft; however, due to the small sample size, this discrepancy may be statistically insignificant.

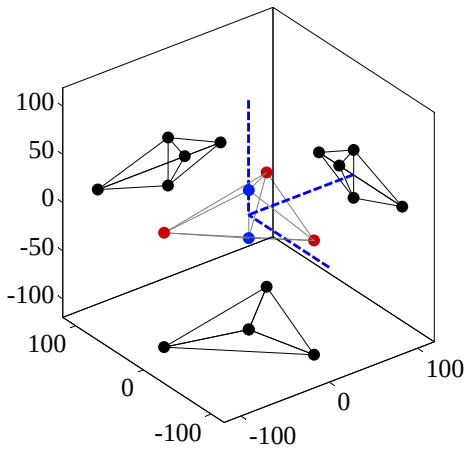

(a) Triangular Five-Craft Formation

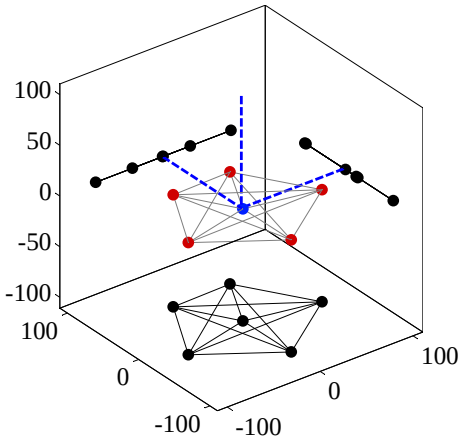

(b) Pentagonal Six-Craft Formation

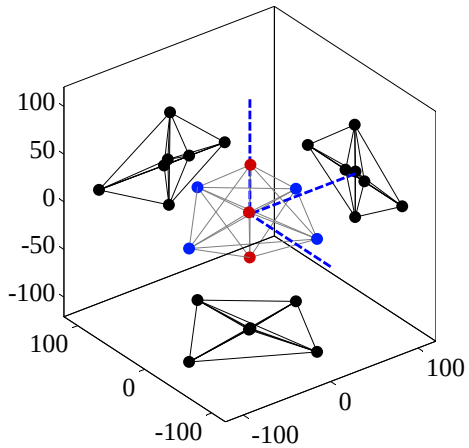

(c) Square Seven-Craft Formation

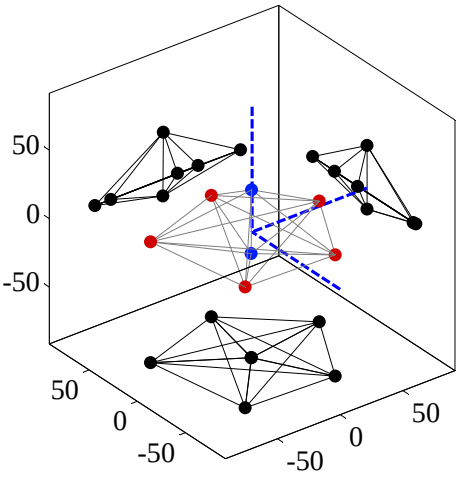

(d) Pentagonal Seven-Craft Formation

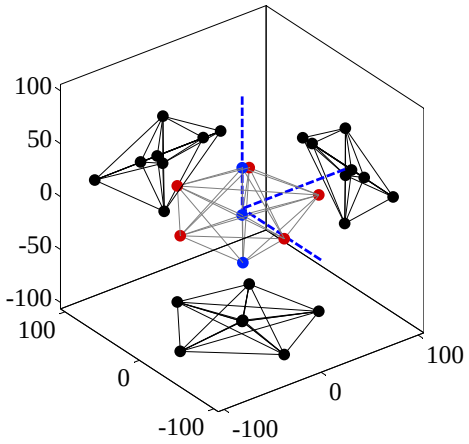

(e) Pentagonal Eight-Craft Formation

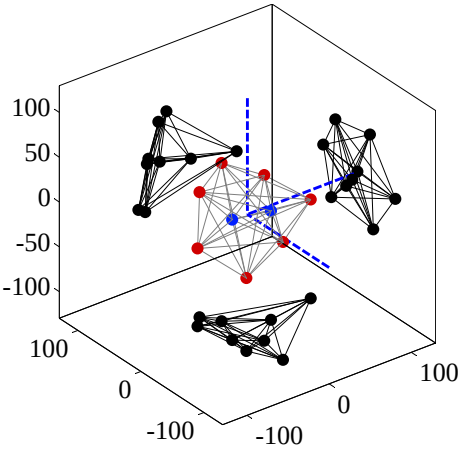

(f) Hexagonal Nine-Craft Formation

Figure 4.7: Examples of deep space formations determined by the GA.

4.3 Numerical Results for Deep-Space Formations.

Early in the research, unreasonably large spacecraft charges – on the order of 1 Coulomb – led to misleading although ultimately useful results. While the formations being produced by the GA were initially assumed to be valid Hill frame formations, the Coulomb interaction of the spacecraft was soon discovered to be so strong that Hill frame accelerations were insignificant in comparison. The problem was immediately corrected, however the "erroneous" initial results were determined to still be valid formations when placed outside of the gravitational influence of Earth. To demonstrate their validity, refer to the complete Hill equations of Eqn. (2.2). In deep space, the Debye length would be extremely large, and the exponential terms in these equations can therefore be safely omitted. In addition, the magnitude of the orbital rate, n is insignificantly small, and can be disregarded when compared with the Coulomb accelerations on the right side of the equation. After prescribing all of the velocities to be zero, the remaining static equations are of the form

$$\ddot{d}_i = 0 = \frac{k_c}{m_i} \sum_{j=1}^{N} \frac{d_i - d_j}{\rho_{ij}^3} q_i q_j \tag{4.12}$$

where d can represent either x, y, or z. The equations represented by Eqn. (4.12) for $i = 1..N$ and for $d = x, y,$ or z can be formed into a matrix equation as follows

$$\underbrace{\begin{bmatrix} 0 \\ 0 \\ \vdots \\ 0 \end{bmatrix}}_{\mathbf{0}} = k_c \underbrace{\begin{bmatrix} \frac{x_1 - x_2}{m_1 \rho_{12}^3} & \frac{x_1 - x_3}{m_1 \rho_{13}^3} & \cdots & \cdots \\ \frac{y_1 - y_2}{m_1 \rho_{12}^3} & \frac{y_1 - y_3}{m_1 \rho_{13}^3} & & \\ \vdots & & \ddots & \\ \vdots & & & \frac{z_{N-1} - z_N}{m_N \rho_{N-1\,N}^3} \end{bmatrix}}_{\boldsymbol{D}} \underbrace{\begin{bmatrix} q_1 q_2 \\ q_1 q_3 \\ \vdots \\ q_{N-1} q_N \end{bmatrix}}_{\mathbf{Q}} \tag{4.13}$$

or simply

$$\mathbf{0} = \boldsymbol{DQ} \tag{4.14}$$

Since the effects of orbital dynamics are insignificant when compared with the large Coulomb interaction of the initial formations, these formations represent solutions to Eqn. (4.14) rather than the Hill frame equations discussed in Chapter 2. By multiplying $\boldsymbol{Q}$ with an arbitrary value, it is immediately apparent that the charging solutions for deep space formations are arbitrarily scalable. Therefore, even though a formation spacecraft would never be charged to potentials as high as 1 Coulomb, the charging solutions for the initial formations are still valid and can be scaled to lower values that can be more reasonably implemented.

Figure 4.7 displays several of the formations that were determined during this initial portion of the research. The three orthogonal axes that are displayed correspond to the principal axes of the formation and the shade of a spacecraft indicates the polarity of the spacecraft's charge. By inspection, these formations are much more symmetric than the

solutions for the Hill frame. The geometry of the majority of the formations between four and nine spacecraft can be qualitatively described by the number of craft that lie on a circle and the number of craft that lie on an axis of symmetry perpendicular to the circle. For instance, the formation in Fig. 4.7(a) has two spacecraft on the axis and three oppositely-charged spacecraft located on a circle in a plane perpendicular to the axis. A more complex formation, Fig. 4.7(e), has three spacecraft on the axis and five oppositely charged spacecraft located on the circle. As the number of spacecraft increases beyond seven, the formations seem to become more disorganized. With greater than nine craft, the formations determined by the GA no longer exhibit axial symmetry. Although this loss of symmetry may be in part due to poor convergence of the genetic algorithm, it could also indicate that no more than three or four craft can be placed on the axis of symmetry and no more than six craft can be placed on a circle perpendicular to this axis. The formation seen in Fig. 4.7(f) is the largest formation discovered that maintains an axis of symmetry.

4.4 Parameter Reduction

The genetic algorithm is a computationally intense form of optimization. With each additional parameter that must be specified, the computation necessary increases exponentially. Therefore, everything possible be done to reduce the number of parameters in the search space. The method that was initially employed to reduce the number of parameters was the enforcement of the center of mass condition. As described in Chapter 2, a unique, static Coulomb formation is only possible if the formation center of mass is located at the origin of the Hill frame. This knowledge makes it possible to reduce the number of parameters that must be specified by three. By knowing the position of all but one spacecraft, the position of the final spacecraft can be determined by the center of mass equation, restated as

$$x_N = -\frac{\sum_{i=1}^{N-1} m_i x_i}{m_n} \tag{4.15}$$

$$y_N = -\frac{\sum_{i=1}^{N-1} m_i y_i}{m_n} \tag{4.16}$$

$$z_N = -\frac{\sum_{i=1}^{N-1} m_i z_i}{m_n} \tag{4.17}$$

A similar method was soon developed to make use of the principal axes condition in reducing the search space further. The basic premise of this method is to randomly remove two of the spacecraft from a newly generated offspring formation and to then reposition them such that the center of mass and principal axes conditions are exactly satisfied. Unfortunately this method exhibited significant flaws that precluded it from being useful in this

research. Often, the new positions required to satisfy both constraints were a great distance from the original position. The effect of this drastic relocation of spacecraft was similar to an extreme mutation, making the constrained member dissimilar to its parents. Quite often, the placements resulting from this parameter reduction method are complex in value, indicating that no craft relocation is capable of satisfying the center of mass and principal axes conditions. In this situation, a new, randomly generated formation is introduced in the place of the old, unconstrainable formation. In either case – distant placement or no possible placement – the offspring generated are radically different from the parent formations. Therefore, the good traits of the parents are not adequately passed on to future generations. As a result, the genetic algorithm is reduced to randomly exploring the search space with little direction.

Thus, an alternative method is developed that successfully incorporates both the center of mass and principal axes conditions to reduce the number of parameters in the search space. This method perturbs the location of each spacecraft using a minimum norm solution so that the center of mass and principal axes conditions are approximately satisfied. In order to find the minimum norm solution, it is necessary to truncate the higher order terms of the principal axes condition so that the resulting equations are linear and easily solvable. The derivation of this method is as follows.

At the beginning of the execution of the genetic algorithm, a population of randomly generated formations is created. Each member of this population is specified by a set of positions, (x_i, y_i, z_i), and charges, q_i. In general, these formations will not satisfy the center of mass or principal axes conditions. However, by moving each craft a certain distance, $(\delta x_i, \delta y_i, \delta z_i)$, it is possible to satisfy these conditions. The following equations express the center of mass and principal axes conditions in terms of the original spacecraft position, (x_i, y_i, z_i), and the necessary change in position, $(\delta x_i, \delta y_i, \delta z_i)$.

The center of mass condition is

$$\left\{ \begin{array}{c} \sum_{i=1}^{N} m_i \left(x_i + \delta x_i\right) \\ \sum_{i=1}^{N} m_i \left(y_i + \delta y_i\right) \\ \sum_{i=1}^{N} m_i \left(z_i + \delta z_i\right) \end{array} \right\} = \left\{ \begin{array}{c} \sum_{i=1}^{N} m_i x_i + \sum_{i=1}^{N} m_i \delta x_i \\ \sum_{i=1}^{N} m_i y_i + \sum_{i=1}^{N} m_i \delta y_i \\ \sum_{i=1}^{N} m_i z_i + \sum_{i=1}^{N} m_i \delta z_i \end{array} \right\} = 0 \tag{4.18}$$

while the principal axes condition is

$$\left\{\begin{array}{l}\sum_{i=1}^{N} m_i\left(x_i+\delta x_i\right)\left(y_i+\delta y_i\right)\\ \sum_{i=1}^{N} m_i\left(y_i+\delta y_i\right)\left(z_i+\delta z_i\right)\\ \sum_{i=1}^{N} m_i\left(z_i+\delta z_i\right)\left(x_i+\delta x_i\right)\end{array}\right\}$$

$$=\left\{\begin{array}{l}\sum_{i=1}^{N} m_i x_i y_i+\sum_{i=1}^{N} m_i x_i \delta y_i+\sum_{i=1}^{N} m_i \delta x_i y_i+\sum_{i=1}^{N} m_i \delta x_i \delta y_i\\ \sum_{i=1}^{N} m_i y_i z_i+\sum_{i=1}^{N} m_i y_i \delta z_i+\sum_{i=1}^{N} m_i \delta y_i z_i+\sum_{i=1}^{N} m_i \delta y_i \delta z_i\\ \sum_{i=1}^{N} m_i z_i x_i+\sum_{i=1}^{N} m_i z_i \delta x_i+\sum_{i=1}^{N} m_i \delta z_i x_i+\sum_{i=1}^{N} m_i \delta z_i \delta x_i\end{array}\right\}=0 \tag{4.19}$$

If the δ terms are small, then the 2nd order terms of Eqn. (4.19) can be omitted. The resulting approximation is

$$\left\{\begin{array}{l}\sum_{i=1}^{N} m_i x_i y_i+\sum_{i=1}^{N} m_i x_i \delta y_i+\sum_{i=1}^{N} m_i \delta x_i y_i\\ \sum_{i=1}^{N} m_i y_i z_i+\sum_{i=1}^{N} m_i y_i \delta z_i+\sum_{i=1}^{N} m_i \delta y_i z_i\\ \sum_{i=1}^{N} m_i z_i x_i+\sum_{i=1}^{N} m_i z_i \delta x_i+\sum_{i=1}^{N} m_i \delta z_i x_i\end{array}\right\}=0 \tag{4.20}$$

Eqs. (4.18) and (4.20) are represented in matrix form as

$$\underbrace{\begin{bmatrix}\sum_{i=1}^{N} m_i x_i\\ \sum_{i=1}^{N} m_i y_i\\ \sum_{i=1}^{N} m_i z_i\\ \sum_{i=1}^{N} m_i y_i z_i\\ \sum_{i=1}^{N} m_i z_i x_i\\ \sum_{i=1}^{N} m_i x_i y_i\end{bmatrix}}_{\mathbf{L}}=-\underbrace{\begin{bmatrix}\{m\}^T & 0 & 0\\ 0 & \{m\}^T & 0\\ 0 & 0 & \{m\}^T\\ 0 & \{mz\}^T & \{my\}^T\\ \{mz\}^T & 0 & \{mx\}^T\\ \{mz\}^T & \{mx\}^T & 0\end{bmatrix}}_{\mathbf{M}}\underbrace{\begin{bmatrix}\{\delta x\}\\ \{\delta y\}\\ \{\delta z\}\end{bmatrix}}_{\mathbf{D}} \tag{4.21}$$

$\{m\}^T=[m_1,m_2,...,m_N]$, $\{md\}^T=[m_1d_1,m_2d_2,...,m_Nd_N]$, and $\{\delta d\}=[\delta d_1,\delta d_2,...,\delta d_N]^T$. Notice that the left hand side of the equation is simply an array of the first moments of

inertia and the products of inertia about the Hill frame origin. Also notice that the matrices in Eqn. (4.21) are denoted $\mathbf{L}$, $\mathbf{M}$, and $\mathbf{D}$ as seen below the underbrace. For an N-craft formation, $\mathbf{L}$ is a $[6\times 1]$ array, $\mathbf{M}$, is a $[6\times 3N]$ matrix, and $\mathbf{D}$ is a $[3N\times 1]$ array. Therefore, for any formation, $\mathbf{D}$ is always longer than $\mathbf{L}$, making it possible to find a minimum norm solution for $\mathbf{D}$ capable of satisfying Eqn. (4.21). The formulation of the solution is simply

$$\mathbf{D}^* = \mathbf{M}^T\left(\mathbf{M}\mathbf{M}^T\right)^{-1}\mathbf{L} \tag{4.22}$$

where $\mathbf{D}^*$ is the minimum norm vector that satisfies Eqn. (4.21). The implementation of this method of parameter reduction in Matlab is straightforward. However, if one intends to take advantage of fast computation inherent with a compiled language such as C, C++, or FORTRAN, it is beneficial to be aware of a method to efficiently invert the $[6\times 6]$ $\mathbf{M}\mathbf{M}^T$ matrix. The matrix $\mathbf{M}\mathbf{M}^T$ is evaluated as

$$\mathbf{M}\mathbf{M}^T = \begin{bmatrix} |m|^2 & 0 & 0 & 0 & m^T\{mz\} & m^T\{my\} \\ 0 & |m|^2 & 0 & m^T\{mz\} & 0 & m^T\{mx\} \\ 0 & 0 & |m|^2 & m^T\{my\} & m^T\{mx\} & 0 \\ 0 & m^T\{mz\} & m^T\{my\} & |my|^2+|mz|^2 & \{mx\}^T\{my\} & \{mz\}^T\{mx\} \\ m^T\{mz\} & 0 & m^T\{mx\} & \{mx\}^T\{my\} & |mz|^2+|mx|^2 & \{my\}^T\{mz\} \\ m^T\{my\} & m^T\{mx\} & 0 & \{mz\}^T\{mx\} & \{my\}^T\{mz\} & |mx|^2+|mz|^2 \end{bmatrix} \tag{4.23}$$

This matrix has several qualities that are beneficial when inverting the matrix. First, this matrix can be divided into four $[3\times 3]$ submatrices.

$$\mathbf{M}\mathbf{M}^T = \left[\begin{array}{c|c} \mathbf{A} & \mathbf{B} \\ \hline \mathbf{B} & \mathbf{C} \end{array}\right] \tag{4.24}$$

The $\mathbf{A}$ matrix is diagonal, and can be trivially inverted. The two $\mathbf{B}$ matrices are symmetric with only off diagonal terms, and computational time can be saved my inverting this relatively simple matrix only once. Finally, the $\mathbf{C}$ matrix is the most difficult to invert, however due to its symmetry, it is still easier to invert than a general, asymmetric $[3\times 3]$ matrix. In terms of these four submatrices, it can be shown that

$$\left(\mathbf{M}\mathbf{M}^T\right)^{-1} = \begin{bmatrix} \mathbf{A}^{-1}+\mathbf{A}^{-1}\mathbf{B}\Delta^{-1}\mathbf{B}\mathbf{A}^{-1} & -\mathbf{A}^{-1}\mathbf{B}\Delta^{-1} \\ -\Delta^{-1}\mathbf{B}\mathbf{A}^{-1} & \Delta^{-1} \end{bmatrix} \tag{4.25}$$

where Δ, the Schur complement, is defined as $\Delta = \mathbf{C}-\mathbf{B}\mathbf{A}^{-1}\mathbf{B}$.[20] Rather than finding the inverse of $\mathbf{M}\mathbf{M}^T$ at each iteration, it may be even more efficient to solve the equation $(\mathbf{M}\mathbf{M}^T)\mathbf{X} = \mathbf{L}$ at each iteration using a method such as Gausian elimination, and in future work this should be investigated more thoroughly.

Now that this method of parameter reduction has been adequately defined, its qualities can be compared with the previous method of parameter reduction. The initial two-craft

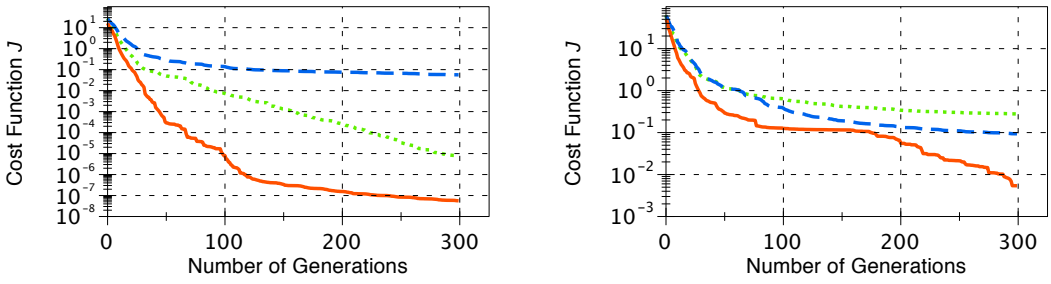

(a) Three-craft search with 85 Runs

(b) 4-Craft search with 20 Runs

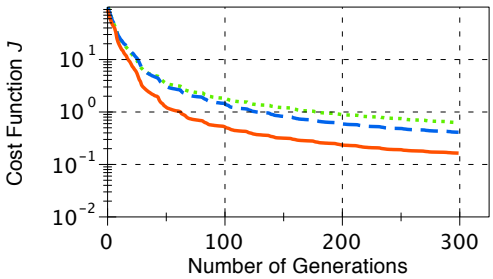

(c) 5-Craft search with 82 Runs

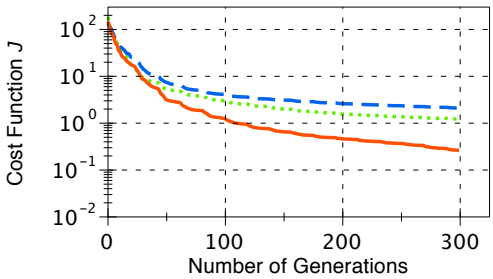

(d) 6-Craft search with 19 Runs

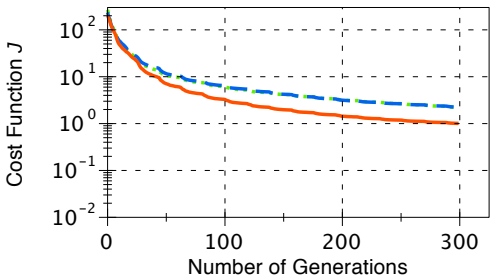

(e) 7-Craft search with 78 Runs

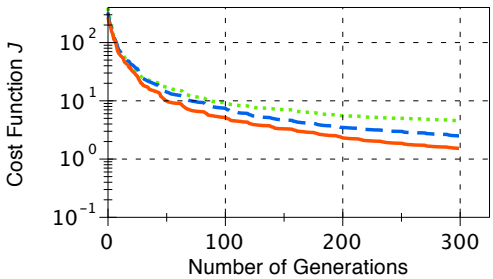

(f) 8-Craft search with 16 Runs

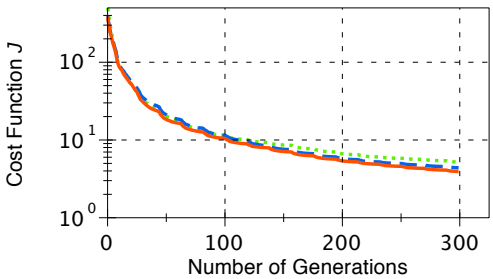

(g) 9-Craft search with 78 Runs

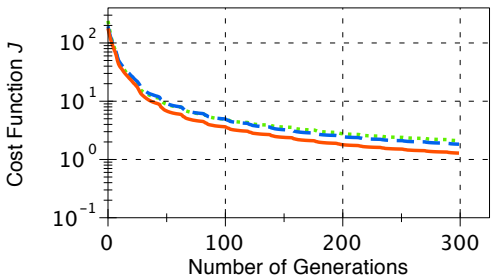

(h) Average Result of all three–9 Craft Searches

Figure 4.8: Genetic search convergence comparisons for the original parameter reduction (· · ·), minimum norm center of mass parameter reduction (- - -), and minimum norm center of mass/principal axes parameter reduction (—).

repositioning technique directly removes six parameters from the search space by making the positions of two craft, (x_i, y_i, z_i) for $i = 1$ and 2, a function of the remaining craft positions. In contrast, the minimum norm technique more subtly removes six parameters by constraining all of the positions to adhere to the three center-of-mass constraints and the three linearized principal axes constraints. As a result, instead of drastically repositioning two of the craft, the position of each craft is changed by a relatively small amount. Therefore the "fittest" parents are able to more coherently pass on their traits to their offspring. In addition, the minimum norm method never produces any degenerate positioning results such as extremely distant or complex-valued positions.

In Fig. 4.8, a comparison is made of the different methods of parameter reduction. The dotted line represents the original center of mass parameter reduction method which directly replaces one spacecraft in order to satisfy the center of mass condition. The dashed line represents a minimum norm version of the center of mass parameter reduction. This method follows the same principle as the center of mass/principal axes minimum norm method except that only the center of mass condition is satisfied. This method is included for the sake of comparison. Finally, the solid red line represents the minimum norm center of mass/principal axes parameter reduction method. Because of its poor performance, the direct two-craft replacement method is not displayed. These plots compare the convergence and convergence rates of all three methods for different size formations. The two center of mass methods tend to be on the same scale as one other while the full center of mass and principal axes method shows a marked improvement. For smaller formations, the center of mass/principal axes method converges several times faster than its competitors. In addition, the final values determined by the center of mass/principal axes method are typically much smaller than the converged values of the other methods. Both the convergence value and the convergence rate attest to the fact that it is beneficial to incorporate both the center of mass and principal axes constraints in the reduction of parameters.

4.5 Extension to Cluster Computing

The results of the numerical analysis presented here are the product of code written in Matlab, a high level scripting language. Although Matlab is ideal for quickly developing and exploring ideas, it is significantly slower than compiled programming languages such as FORTRAN, C, or C++. For this reason, it is desirable to export the genetic algorithm from Matlab to one of these languages in order to take advantage of the inherent speed of a compiled language. However, the genetic algorithm is exceptionally computationally intense, and certain applications that lie in the future of Coulomb formation research will require an even greater source of computational power - massive cluster computing. Such applications may include the determination of static N-craft formations for large N, the determination of dynamic periodic formations, and the determination of the motion and interactions of Coulomb spacecraft modeled as rigid bodies of finite size rather than infinitesimal point

charges. This section discusses several possible implementations of the genetic algorithm over a cluster of computers.

A common template used to take advantage of cooperative cluster processing is the master/slave paradigm. In a typical master/slave program, once the program begins execution on the cluster, each computing node will first determine its role. One node will be chosen to be the master while the remainder of the nodes will become slaves. The role of the master is to divide the work into smaller portions, send work to the slaves, and then to receive the completed work and organize the results. The task of the slave, accordingly, is to receive the packets of work from the master, process the information, and then return the results back to the master. Therefore, the majority of the computational load is put upon the slave. Once all tasks are completed, the master node broadcasts the command to quit working and cleanup all processes. At this point, the execution of the cluster program terminates.

With the genetic algorithm, the fitness evaluation is often the most computationally intense portion of the algorithm. Therefore, one of the simplest methods that can be employed to take advantage of the master/slave concept is to allow the slave nodes to determine the fitness of each member. In this implementation, the master would create randomly generated parent formations and then send them in pairs to the slave nodes. The slave nodes in turn would be responsible for mating these parents, and then mutating, and constraining the offspring as need be. Once this task is complete, the slave nodes evaluate the fitness of the offspring and then return the offspring with it's fitness value to the master. The master receives the new offspring, sorts it into the population according to fitness, destroys the weakest member of the population, and then sends two new parent formations to the slave that just completed its work. This cycle continues until the algorithm converges to a solution or until the fitness criteria is met. This method is illustrated in Fig. 4.9. Unlike the single processor version of the genetic algorithm which mates, and sorts an entire population at once, this version of the GA continuously mates members, sorts the offspring into the population, destroys the weakest members. The result is a fluid concept of population that more closely mimics the changes of populations in living organisms. Despite these attractive qualities, this method was determined to be infeasible. In a simulation of this algorithm in Matlab, the population would most often converge to non-optimal solutions. In addition, there are communication issues that would become important when implementing this algorithm over a network of computers. When transmitting a small amount of information, in this case the genetics and fitnesses of a couple of members, there is a tremendous communication overhead. For a larger cluster, the slaves would likely finish their work well before the master is ready to receive it.

In response to these issues, a similar method is considered which improves upon the shortcomings of the method just described. In order to mitigate problems with the communication overhead, the slave nodes are given entire populations rather than single members of the population. In this case, the slave nodes perform a single iteration of the genetic algorithm by mating the members of their population, mutating and constraining the off-

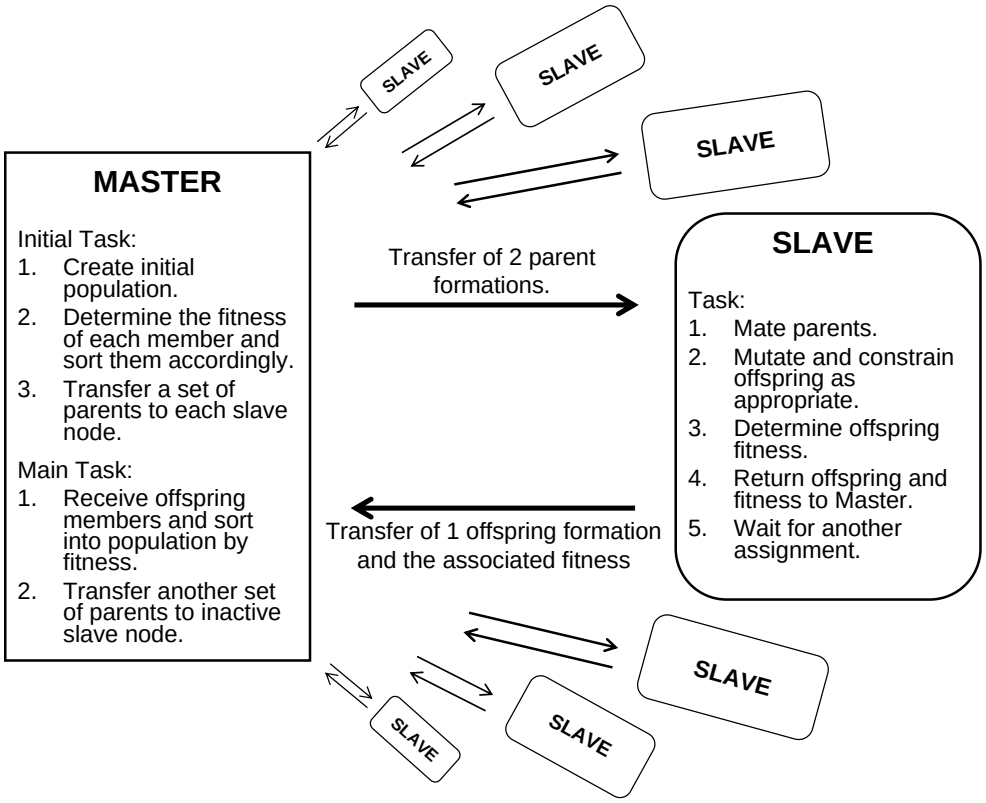

Figure 4.9: Single member method for distributing the genetic algorithm.

spring as necessary, determining the fitness of each offspring, and then sorting the offspring into the population according to fitness. This method is illustrated in Fig. 4.10. In this algorithm there may be instances when master is forced to wait until the slaves complete their work, but it is much better to have one master waiting on 99 slaves than to have 99 slaves waiting on one master. Before attempting to implement this algorithm in a computer cluster, this algorithm was first simulated in Matlab. Unlike the previous method which quickly converges to poor solutions, this method proves to be much more robust. Because of its superior performance, this latter method has been selected for implementation using the Message Passing Interface protocol, (MPI). In the future, the genetic algorithm will be applicable not only to static formation determination, but to a number of other research interests.

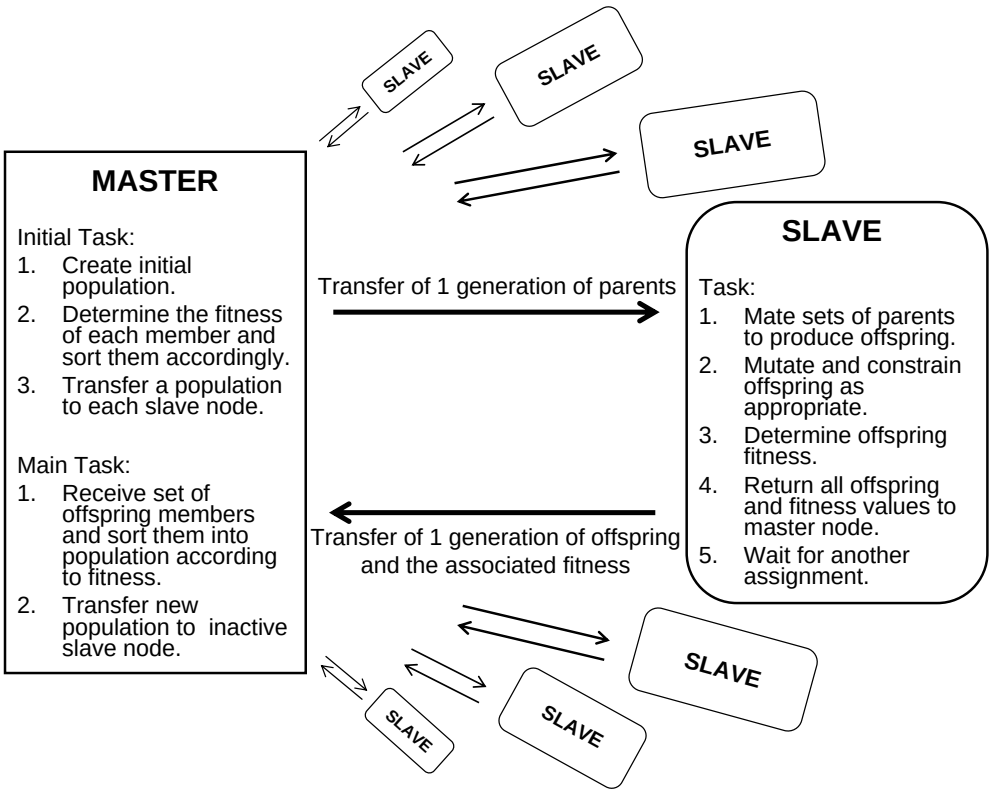

Figure 4.10: Full population method for distributing the genetic algorithm.

Chapter 5

Conclusions and Future Work

For close proximity flying, Coulomb-controlled formations offer an exciting alternative to other candidate propulsion systems. In addition to lower weight and better fuel efficiency, Coulomb control is essentially propellantless and is therefore much less likely to damage formation spacecraft due to plume impingement. If sufficiently developed, this technology may provide a reliable and inexpensive method of formation control with applications ranging from sparse aperture telescopes to virtual space structures or Coulomb tethers.

In this thesis, both analytical and numerical analyses are presented. The analytical work reveals several important results leading to a better understanding of the nature of static Coulomb formations. Specifically, a method is derived in which the charge products, Q_{ij}, can be determined for any constant charge formation. The charge products are then related to the charges necessary to maintain a static Coulomb formation, $\tilde{q}_i$. Since it is *not* always possible to find real, single-valued charges, a criterion is developed to indicate if a given formation is implementable based upon the charge products determined for that formation. Once constant charges have been successfully determined for a formation, they can be used as open-loop feed-forward charges in stabilizing feedback control laws. Further in the analytical portion of this thesis, the interrelation between constraint conditions and static equations is discussed. It is shown that the center of mass and principal axes conditions can be employed to eliminate six of the static equations for the case of a general three-dimensional formation. Finally, examples are supplied for specific formations including linear two- and three- craft formations, and equilateral triangle formations.

In the numerical analysis, a genetic algorithm is developed for the purpose of determining static formations for a given number of craft. A detailed description of this algorithm is provided, including special attention to the structure of the fitness function and methods to reduce the dimensionality of the search space. The formations resulting from the genetic algorithm confirm the analytical results and give additional insight into the qualitative nature of Coulomb formations of more than three spacecraft.

Although in its infancy, the study of Coulomb formation statics and dynamics has proven to be a rich field of research. Coulomb formations may hold answers to many of the logistical concerns that plague close proximity flying today.[1] However, with each question that is answered, several more interesting questions arise. Future research will therefore be directed toward many different areas. One avenue of research will be the determination of the controllability and stability of different Coulomb formations. During this work it is shown that constant charges are incapable of controlling certain formations. However, it seems plausible that a method known as pulse-width modulation may be used to overcome this problem by rapidly pulsing the spacecraft charges on and off and thereby producing appropriate inter-craft forces. In this research, the spacecraft are assumed to be point masses and point charges. These assumptions break down for small separation distances or for sufficiently large spacecraft. To this end, research is currently underway to determine the differences between the Coulomb interaction of point charges and the Coulomb interaction of charged bodies. One of the assumptions made during this current research is that the Debye length is large enough to allow the exponential Coulomb force decay term to be disregarded. Future work will extend the analysis to include consideration of formations in orbits lower than GEO where it will be impossible to omit the exponential term. Also, although the formations considered in this work are all static, it should be possible to have dynamic formations with patterns that repeat periodically. As the research moves from static to dynamic formations and to an increased number of spacecraft, the computational requirements will greatly increase. Expanding the genetic algorithm to a distributed computing platform will help accommodate the demands of future research.

Bibliography

[1] King, Lyon B., Parker, Gordon G., Deshmukh, Satwik, et al., "Spacecraft Formation-Flying using Inter-Vehicle Coulomb Forces", Tech. rep., NASA/NIAC, January 2002, `http://www.niac.usra.edu`.

[2] King, Lyon B., Parker, Gordon G., Deshmukh, Satwik, et al., "Study of Interspacecraft Coulomb Forces and Implications for Formation Flying", *AIAA Journal of Propulsion and Power*, Vol. 19, No. 3, May–June 2003, pp. 497–505.

[3] Torkar, K. and et. al., "Active Spacecraft Potential Control for Cluster – Implementation and First Results", *Annales Geophysicae*, Vol. 19, 2001, pp. 1289–1302.

[4] Schaub, Hanspeter, Parker, Gordon G., and King, Lyon B., "Challenges and Prospect of Coulomb Formations", *AAS John L. Junkins Astrodynamics Symposium*, College Station, TX, May 23-24 2003, Paper No. AAS-03-278.

[5] Chong, Jer-Hong, *Dynamic Behavior of Spacecraft Formation Flying using Coulomb Forces*, Master's thesis, Michigan Technological University, May 2002.

[6] Schaub, Hanspeter, "Stabilization of Satellite Motion Relative to a Coulomb Spacecraft Formation", *AAS Space Flight Mechanics Meeting*, Maui, Hawaii, Feb. 8–12 2004.

[7] Natarajan, Arun and Schaub, Hanspeter, "Linear Dynamics and Stability Analysis of a Coulomb Tether Formation", *AAS Space Flight Mechanics Meeting*, Copper Mountain, CO, Jan. 23–27 2005, paper No. AAS 05–204.

[8] Mullen, E. G., Gussenhoven, M. S., and Hardy, D. A, "SCATHA Survey of High-Voltage Spacecraft Charging in Sunlight", *Journal of the Geophysical Sciences*, Vol. 91, 1986, pp. 1074–1090.

[9] Schaub, Hanspeter and Parker, Gordon G., "Constraints of Coulomb Satellite Formation Dynamics: Part I – Cartesian Coordinates", *Journal of Celestial Mechanics and Dynamical Astronomy*, 2004, submitted for publication.

[10] Schaub, Hanspeter and Kim, Mischa, "Orbit Element Difference Constraints for Coulomb Satellite Formations", *AIAA/AAS Astrodynamics Specialist Conference*, Providence, Rhode Island, Aug. 2004, paper No. AIAA 04-5213.

[11] Schaub, Hanspeter, Hall, Christopher, and Berryman, John, "Necessary Conditions for Circularly-Restricted Static Coulomb Formations", *AAS Malcolm D. Shuster Astronautics Symposium*, Buffalo, NY, June. 12–15 2005, paper No. AAS 05–472.

[12] Parker, Gordon G., Passerello, Chris E., and Schaub, Hanspeter, "Static Formation Control using Interspacecraft Coulomb Forces", *2nd International Symposium on Formation Flying Missions and Technologies*, Washington D.C., Sept. 14–16, 2004 2004.

[13] Ferringer, Matthew P. and Spencer, D.B., "Satellite Constellation Design Optimization via Multiple-Objective Evolutionary Computation", *AIAA/AAS Astrodynamics Specialist Conference*, Lake Tahoe, California, Aug. 2005, paper No. AAS 05-280.

[14] Peterson, Glenn E., Campbell, Eric T., McVey, John P., et al., "Genetic Algorithms for Interplanetary Continuous Thrust Trajectory Design", *AIAA/AAS Astrodynamics Specialist Conference*, Lake Tahoe, California, Aug. 2005, paper No. AAS 05-391.

[15] Carnelli, Ian, Dachwald, Bernd, Vasile, Massimiliano, et al., "Low-Thrust Gravity Assist Trajectory Optimization Using Evolutionary Neurocontrollers", *AIAA/AAS Astrodynamics Specialist Conference*, Lake Tahoe, California, Aug. 2005, paper No. AAS 05-374.

[16] Igarashi, J. and Spencer, D.B., "Optimal Continuous Thrust Orbit Transfer Using Evolutionary Algorithms", *Journal of Guidance, Control and Dynamics*, Vol. 28, 2005, pp. 547–549.

[17] Kim, Y.H. and Spencer, D.B., "Optimal Orbital Rendezvous Using Genetic Algorithms", *Journal of Spacecraft and Rockets*, Vol. 39, 2002, pp. 859–865.

[18] Hill, George William, "Researches in the Lunar Theory", *American Journal of Mathematics*, Vol. 1, No. 1, 1878, pp. 5–26.

[19] Clohessy, W. H. and Wiltshire, R. S., "Terminal Guidance System for Satellite Rendezvous", *Journal of the Aerospace Sciences*, Vol. 27, No. 9, Sept. 1960, pp. 653–658.

[20] Schaub, Hanspeter and Junkins, John L., *Analytical Mechanics of Space Systems*, AIAA Education Series, Reston, VA, October 2003.

[21] Berryman, John and Schaub, Hanspeter, "Analytical Charge Analysis for 2- and 3-Craft Coulomb Formations", *AAS/AIAA Astrodynamics Specialist Conference*, Lake Tahoe, CA, August 7–11 2005, paper No. AAS 05–278.

[22] "Mathworld – Complete Graph", 2005, `http://mathworld.wolfram.com/CompleteGraph.html`.

Appendix

Tables 1 and 2 list the positions and charges of several formations presented in this Thesis.

Table 1: Static Hill-frame Coulomb formations with N satellites.

Description	Sat No.	x_i [m]	y_i [m]	z_i [m]	$\tilde{q}_i$ $[C\frac{\sqrt{k_c}}{n}]$
2 Spacecraft	1	-0.092664	0.011066	17.8917	166.7136
Formation	2	0.092664	-0.011066	-17.8917	136.896
3 Spacecraft Linear	1	-0.023484	-0.075065	0.7652	37.4897
Formation ($\hat{\boldsymbol{o}}_h$ aligned)	2	-0.024972	-0.51724	16.7249	-206.2658
	3	0.048456	0.59231	-17.4901	-266.0775
3 Spacecraft Linear	1	-0.036273	21.4974	-0.26514	-175.3544
Formation ($\hat{\boldsymbol{o}}_\theta$ aligned)	2	0.18339	-0.41802	0.11892	42.0475
	3	-0.14712	-21.0794	0.14622	-161.5587
3 Spacecraft Triangular	1	-4.4331	-0.60236	-15.151	-77.022
Formation	2	14.6396	0.1004	3.4265	109.706
(Perpendicular to $\hat{\boldsymbol{o}}_\theta$)	3	-10.2065	0.50196	11.7245	-237.0545
3 Spacecraft Triangular	1	11.6585	3.0029	-0.12805	105.9299
Formation	2	-7.7367	13.8648	-0.30896	-128.7732
(Perpendicular to $\hat{\boldsymbol{o}}_h$)	3	-3.9218	-16.8678	0.43701	-101.1125
7 Spacecraft	1	5.2046	1.2553	7.1177	-34.5258
Formation	2	-0.8901	-19.8049	-0.26195	34.5104
	3	-1.4872	12.6487	-0.82082	13.4644
	4	-5.6985	1.5323	-6.5856	40.5746
	5	1.8194	0.7205	0.31747	-3.997
	6	-5.5185	1.7321	6.7684	40.3356
	7	6.5702	1.916	-6.5351	-54.7031
6 Spacecraft	1	-3.6757	-8.7775	4.7316	18.6585
Formation	2	-4.9418	14.7365	0.032367	31.8215
	3	4.9927	14.9707	-0.31142	-41.7238
	4	-5.3036	-5.8118	-3.7998	39.6514
	5	4.2763	-10.394	-4.6351	-30.5965

Continued on next page

Table 1 – continued from previous page

Description	Sat No.	x_i [m]	y_i [m]	z_i [m]	$\tilde{q}_i$ $[C\frac{\sqrt{k_c}}{n}]$
	6	4.6521	-4.7239	3.9824	-34.3029
6 Spacecraft	1	-0.30092	10.2766	0.69744	26.2459
Formation	2	-0.44629	-13.1755	7.1652	42.4876
	3	1.6249	-1.8444	-0.5891	-30.4786
	4	-0.19733	9.4761	-10.2863	43.6042
	5	-0.47352	-13.3682	-6.6336	42.4052
	6	-0.20681	8.6353	9.6464	24.5486
9 Spacecraft	1	-5.5614	2.5774	-0.27129	-22.9893
Formation	2	4.235	3.3704	-0.42808	-17.4779
	3	-0.27082	3.4834	-0.18405	9.2982
	4	-0.1535	-2.1963	-4.9073	24.1564
	5	-0.68204	-10.8544	0.61756	18.562
	6	-0.13938	-1.986	0.21305	4.536
	7	2.7537	-6.8262	0.27898	-11.1816
	8	-0.0029009	14.5789	-0.58875	70.537
	9	-0.17873	-2.1472	5.2699	21.4357

Table 2: Static deep-space Coulomb formations with N satellites.

Description	Sat No.	x_i [m]	y_i [m]	z_i [m]	$\tilde{q}_i$ $[C\frac{\sqrt{k_c}}{n}]$
5 Spacecraft	1	0.29037	-0.123	25.5215	-0.16283
Triangular	2	-79.3421	21.0519	-0.40555	0.57287
Formation	3	0.22932	-0.057902	-24.2428	-0.17325
	4	59.6878	51.0369	-0.42713	0.50861
	5	19.1346	-71.9079	-0.44602	0.43973
6 Spacecraft	1	-32.4301	53.2384	0.0015872	0.22958
Pentagonal	2	0.64873	-69.3038	-0.0021919	0.26269
Formation	3	-71.9544	-19.4657	0.00085719	0.48613
	4	73.7379	-17.2015	0.0028181	0.50839
	5	0.11216	-2.1257	4.8976e-005	-0.44919
	6	29.8857	54.8583	-0.0031197	0.22838
7 Spacecraft	1	63.7586	14.2322	-2.3797	-0.55481
Square	2	23.0271	-70.4036	-2.0149	-0.79334
Formation	3	1.0453	0.42685	51.1106	0.19367
	4	-1.4587	-0.64427	2.5688	0.44347
	5	-80.3256	-14.015	-1.5827	-0.98964

Continued on next page

Table 2 – continued from previous page

Description	Sat No.	x_i [m]	y_i [m]	z_i [m]	$\tilde{q}_i$ $[C\frac{\sqrt{k_c}}{n}]$
	6	-5.8624	70.5186	-2.2059	-0.70582
	7	-0.18431	-0.11474	-45.4962	0.27081
7 Spacecraft	1	-55.0917	33.6149	-3.2771	0.7888
Pentagonal	2	-42.4004	-48.1463	-3.2575	0.76196
Formation	3	-0.91921	-0.22686	-15.3361	-0.68751
	4	-0.51575	-0.21477	31.0602	-0.34628
	5	10.7419	56.2356	-2.8658	0.45889
	6	27.1891	-50.9637	-2.951	0.48066
	7	60.9961	9.7012	-3.3727	0.77246
8 Spacecraft	1	-23.3827	56.705	3.6453	0.55434
Pentagonal	2	41.2039	44.1073	3.9888	0.56956
Formation	3	-0.61836	-0.83852	-5.5092	-0.52944
	4	-6.3181	-64.8159	3.3862	0.62763
	5	-0.37873	-0.59229	38.9169	-0.44769
	6	0.96295	0.28432	-51.5618	-0.24655
	7	-70.6859	-8.9428	3.2269	0.93987
	8	59.2168	-25.9071	3.9069	0.72482
9 Spacecraft	1	-21.0591	48.481	9.9513	0.2359
Hexagonal	2	-33.2097	35.7212	-42.8278	0.78329
Formation	3	-24.8719	-30.8591	-48.1975	0.42639
	4	30.6973	2.4986	-8.1589	-0.40772
	5	0.92225	-25.6601	55.1498	0.52915
	6	-8.8662	29.3598	46.9042	0.43376
	7	86.4228	12.0836	-19.3785	0.28282
	8	-22.8694	-5.6958	4.7316	-0.75998
	9	-7.166	-65.9292	1.8258	0.6722